Multifunctional structures with quasi-solid-state Li-ion battery cells and sensors for the next generation climate neutral aircraft

Horizon Europe | HORIZON-CL5-2021-D5-01-05

Greenhouse gas aviation emissions reduction technologies towards climate neutrality by 2050

D3.1 – Interim report on structural integration concepts

This project receives funding from the European Union's Horizon Europe research and innovation programme under grant agreement no. 101056674 (MATISSE)

Deliverable No.	D3.1	
Deliverable Title	Interim report on structural integration concepts	
Deliverable Type	Report	
Dissemination level	Sensitive	
Written By	Ignazio Dimino (CIRA), Frederic Laurin (ONERA), Alejandro Treceño Fernández (PVS), Alexander Beutl (AIT); Roberto Simmarano (SCP), Helmut Kühnelt (AIT)	30.06.2023
Checked by	Ignazio Dimino (CIRA)	30.06.2023
Approved by	Helmut Kühnelt (AIT)	15.09.2023
Status	Final	15.09.2023

REVISION HISTORY

Version	Date	Who	Change
A00	30.06.2023	I. Dimino, F. Laurin	Draft
A01	15.09.2023	All	Final

TABLE OF CONTENTS

TABLE OF FIGURES

PROJECT ABSTRACT

MATISSE responds to the fourth bullet of the HORIZON-CL5-2021-D5-01-05 topic “expected outcome”, delivering improved aircraft technologies in the area of multifunctional structures capable of storing electrical energy for hybrid electric aircraft applications. This consists in integrating Li-ion cells into aeronautical composite structures, sharing the load-bearing function with the structure and achieving an aircraft structural element capable of functioning as a battery module.

To do so, MATISSE will:

- advance Li-ion battery cell technology, in a non-conventional formulation suitable for bearing structural loads: NMC811 (cathode), Si/C (anode) and bicontinuous polymer-ionic quasi-solid-state electrolyte (BCE), i.e. NMC811|BCE|Si/C, achieving 170-270 Wh/kg at cell level;
- enable the functional integration of Li-ion cells into solid laminate and sandwich composite structures;
- make the structural battery smart, by equipping it with on-cell and in-structure sensors, connected to a chip-based CMU (Cell Monitoring Unit) and PLC (Power Line Communication).

MATISSE delivers a multifunctional structure demonstrator capable of power delivery, power management and safety monitoring. This consists of a full-scale wing tip (1.42 m × 0.69 m) for use in place of the current wingtip assembly installed on Pipistrel Velis Electro, embedding a module of 40 battery cells at 72 VDC. This will undergo a comprehensive testing and characterisation campaign, qualifying the technology at TRL 4 at the end of the project (2025). MATISSE will also encompass aspects related to flight certification, life-cycle sustainability and virtual scale-up, paving the way towards the application of structural batteries as an improved performance key enabling technology for next generation commuter and regional hybrid electric aircraft applications.

The strong and complementary consortium of 8 partners from 5 different European countries and one associated partner country representing industrial companies, SMEs and RTOs is coordinated by AIT Austrian Institute of Technology. MATISSE is scheduled to run from September 1st 2022 to August 31st 2025, for a total duration of 36 months and has received funding from the European Union’s Horizon Europe research and innovation programme under Grant Agreement no. 101056674. A full list of partners and funding can be found at: https://cordis.europa.eu/project/id/101056674.

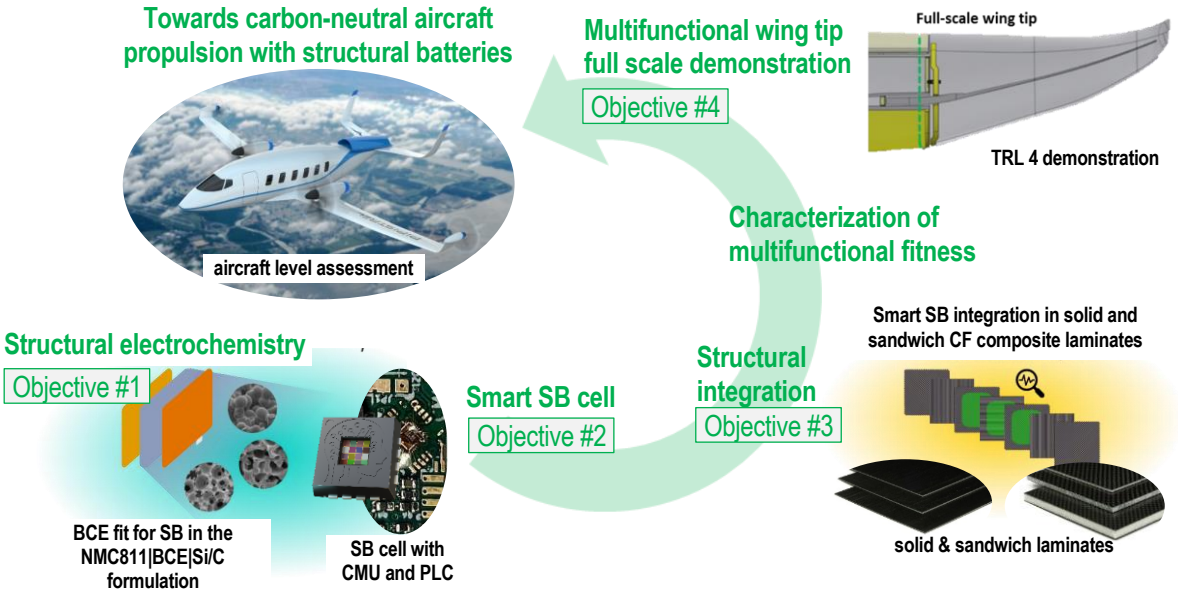

Figure 1 – MATISSE concept overview (graphical abstract)

LIST OF ABBREVIATIONS

Acronym / Short Name	Meaning
CF (RP)	Carbon fiber (reinforced polymer)
CMU	Cell monitoring unit
RMS	Reinforced Multilayer Stack
SB	Structural battery
SPLC	Sensichips Power Line Communication system

EXECUTIVE SUMMARY

The MATISSE project addresses advanced multifunctional aeronautical structures by integrating solid battery cells into composite and sandwich laminates. Combining load bearing functions and energy storage capabilities require novel design tools and simulation approaches capable to estimate both the electrochemical storage capacity the decreased mechanical performance.

The objective of this deliverable is to provide an interim assessment of structural integration concepts and related design methodologies developed in MATISSE to evaluate the effect of structural battery integration on the mechanical properties of both CFRP solid and sandwich laminates. An integrated design process is developed and preliminary tested on the same composite material (meaning AS4/8552) used in SOLIFLY. The related low-velocity damage mechanism is also investigated on both laminate and sandwich structures to preliminary assess the influence of battery packs, considering the lack of accepted test methods and data available in the literature. The main challenge is both to simulate the damage during impact and to predict the mechanical characteristics after impact, in order to be able to numerically optimize the design of such multifunctional structures with the right impact damage tolerance.

The influence of the battery integration into composite laminated plates is predicted on the global rigidity, the onset of damage but also on the damage evolution and final failure. The design methodology is implemented by ONERA in Abaqus/Explicit, same finite element solver used by CIRA, and developed to consider the different damage and failure mechanisms such as transverse cracks, delamination and fibre failure. The proposed modelling approach is validated on a sample manufactured and successfully tested by ONERA. Furthermore, preliminary impact simulations are performed in accordance to the standard ASTM 7136, since no other specific standard are available. Low impact energy cases are studied to predict battery damage when the surface is still intact or not visible damaged. The introduction of a core between the two composite plates is modelled along with the embedded structural batteries in order to increase the overall bending stiffness of the sandwich laminate and therefore improve its final buckling characteristics.

1. INTRODUCTION

Electrification of aircraft systems is key for increasing efficiency and reducing climate impact of air transport towards the European net-zero goal. The functional integration of structural capabilities and electrical energy storage in the form of structural batteries (SB) is considered as a low TRL technology with the potential to reduce the impact of battery energy storage on the overall aircraft weight. So far, structural batteries have been mainly studied at material level, largely neglecting their integration into aircraft structures. The HORIZON project MATISSE is developing further structural batteries for aeronautical applications, representative of industrial composite parts. Starting from the concepts developed in CS2 SOLIFLY [1,2], the project puts particular emphasis on their integration into both CFRP monolithic and sandwich laminates within an aeronautical demonstrator (TRL 4). To this aim, advanced simulations are carried out at coupon level in WP3 in order to predict their mechanical performance and investigate the low velocity/low energy impact behaviour. The demonstrator design, manufacturing and testing (WP5) as well as the virtual upscale of the MATISSE multifunctional energy storage to aircraft level (WP6) will pave the way for commercialization, in the long term, of structural batteries in commuter and regional size vehicles.

1.1. SCOPE OF THE DELIVERABLE

The purpose of D3.1 “Interim report on structural integration concepts” is to provide an interim evaluation of the integrated design process developed in MATISSE to investigate structural integration concepts of smart SB cells into solid and sandwich laminates.

This report presents design, modelling and simulation results of structural integration concepts for both CFRP solid and sandwich laminates. The effect of structural battery integration is firstly studied on the mechanical properties of CFRP solid laminates, by considering the size and shape of the structural battery insert as well as its location through the laminate thickness. Moreover, an automatic procedure is developed to integrate battery cells into both the face sheets and the core of sandwich structures. Low velocity/low energy impact tests are finally simulated on both solid and sandwich laminates to determine how the integration of SB cells decreases the related impact resistance. The structural design approach and related numerical models developed in this work packages will be then validated against the experimental data acquired in WP4.

2. STRUCTURAL BATTERIES

The MATISSE project focuses on the development of a mature and robust structural battery concept, as reported in Figure 2. The multifunctional Reinforced Multilayer Stack (RMS) SB cell consists of conventionally coated anode on Cu foil and cathode on Al foil. The electrolyte consists of a polymer which provides mechanical stiffness and strength and a liquid electrolyte for ion conduction. No additional separator is needed. The thickness of a battery cell is matching the thickness of one or more CF plies with a weight areal per ply around 200g/m^2, allowing many possibilities for the integration of battery cells in composite parts.

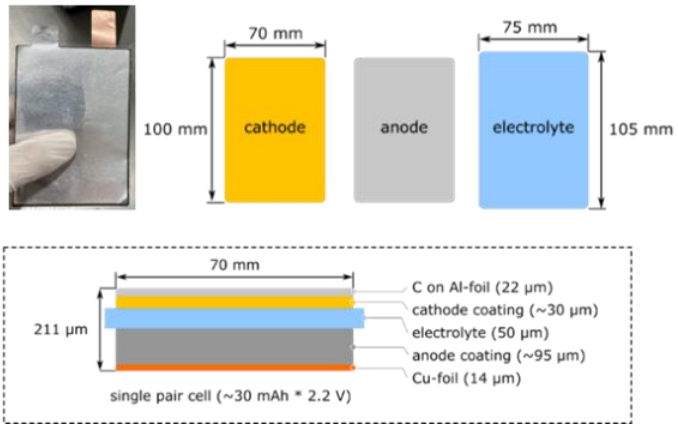

Figure 2: Presentation of the RMS structural battery cell concept and preliminary cell layup considered in MATISSE project

A series of electrodes (NMC cathode, composited NMC cathode, Si/graphite anode, and composited graphite anode) with different electrolytes (gel electrolyte, and hybrid electrolyte) are being investigated in the framework of WP 2.

The initial electrochemical performance of multi-layer pouch cells developed within the project are detailed in Deliverable D2.1 “Interim report on electrochemical material selection, initial cell design, on-cell sensor development “ [3], along with safety and repeatability issues during cell scale-up. In addition, the incorporation of the CMU-I unit and SPLC system in the multi-layer pouch cells is also in progress.

3. STRUCTURAL INTEGRATION CONCEPTS – SOLID LAMINATES

3.1. DESIGN METHODOLOGY

In the European SOLIFLY project, ONERA has developed a methodology to estimate the decrease of the mechanical properties (macroscopic rigidity and onset of damage) of a laminated composite plate due to the integration of solid battery cells within the coupon in order to establish some recommendations for the design and manufacturing [2].

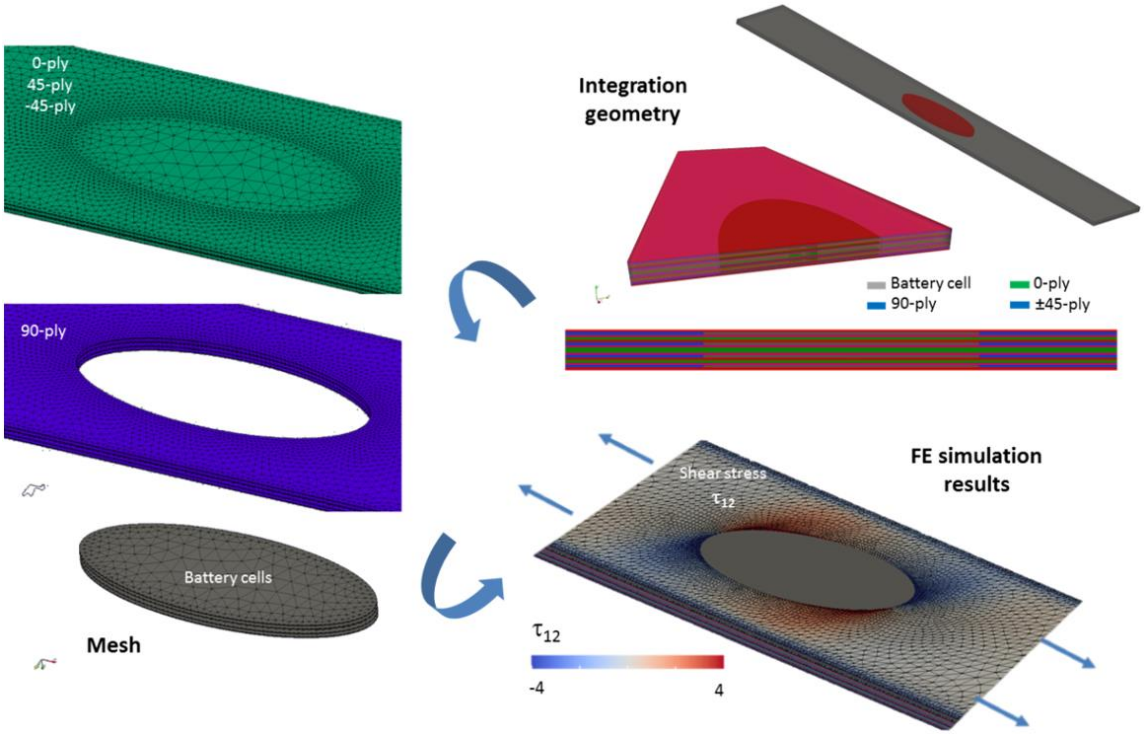

Figure 3: Numerical strategy for the cell integration concept for solid laminate composites (developed in SOLIFLY)

The numerical strategy is illustrated on a quasi-isotropic $[(45/90/-45/0)_2]_s$ laminate as reported in Figure 3. The battery cells are explicitly introduced into the finite element simulation within composite laminates subjected to tensile or compressive or bending loadings, which are the relevant ones when considering industrial composite structures. The battery cell has a thickness approximately corresponding to that of a UD ply or multiples thereof (around 0.2 mm per ply) and can therefore be easily integrated into the stacking sequence as a part of the ply. It should be noted that the cell thickness of the RMS concept can be adjusted to match the ply thickness by adapting the thicknesses of the cathode and anode coating. The finite element simulations are performed with the in-house software Z-set developed jointly by ONERA and the Ecole des Mines, using an implicit solver. The boundary conditions applied to the FE simulations consist of fixing the lower free edge and imposing the uniaxial displacement on the upper free edge at a constant displacement rate. Finite element simulations are considered without geometric non-linearities due to the low strain at failure of the carbon/epoxy laminates considered. The finite element simulations are performed considering linear elastic behaviour for the composite material and for the battery cells. The composite plies are assumed to be perfectly bonded to each other but also to the battery cells, which is an arguable assumption made for the sake of simplicity. In order to estimate the onset of damage in the composite material, the ONERA

Progressive Failure Model (OPFM), which has been validated on many test configurations for carbon/epoxy laminates [4], was used as a post-processing to the linear elastic simulations at each Gauss point.

In the MATISSE project, considering the final demonstrator proposed by Pipistrel, it is important to be able to predict the influence of the battery integration on the global rigidity, the onset of damage but also on the damage evolution and, more importantly, on the final failure. For that reason, the methodology previously developed at ONERA has been implemented in Abaqus/Explicit, same finite element solver used by CIRA in the MATISSE project, and extended to consider the different damage and failure mechanisms such as transverse cracks, delamination and fibre failure. As reported in Figure 4, the battery cells are still explicitly integrated in the mesh considering C3D8R solid elements for the battery cells and the composite plies (one element through the thickness of the ply) and COH3D8 cohesive elements are introduced between plies with different orientations. No cohesive element has been introduced at the interfaces between the battery cells.

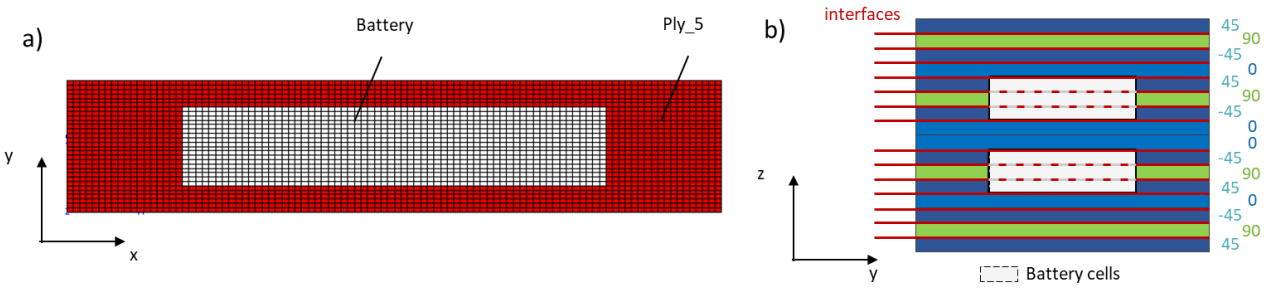

Figure 4: Integration of battery cells in simulations performed with Abaqus/explicit in a 16 plies quasi-isotropic laminate

The damage and failure approach developed at ONERA called Onera Progressive Failure Model (OPFM) has been implemented in VUMAT. A non-linear thermo-viscoelastic behaviour has been proposed and is reminded in Eq. 1.

$$\sigma = C^{eff} : (\varepsilon - \varepsilon^{ve} - \varepsilon^{nl}) \quad (1)$$

where σ is the mesoscopic stress, C^{eff} the effective stiffness, ε the total strain, ε^{nl} the non-linear elastic strain (in order to describe the hardening observed experimentally on UD plies subjected to longitudinal tensile loading and in particular on new generations of composites), and ε^{ve} the viscous strain (to take into account the non-linearity observed on UD plies subjected to shear loading, which is essential for accurate prediction of cracks in ±45 plies). Secondly, the prediction of the ply failure within the laminate is performed with a failure criterion, based on Hashin's hypotheses [5], distinguishing the fibre failure mode and the in-plane interfibre failure and modelling the failure mechanisms in tension and in compression separately for each failure mode. The main improvement of the interfibre failure criterion, over the Hashin criterion, is a better description of the reinforcement of the apparent strength of the material for combined in-plane shear and transverse compressive loadings. Thirdly, when transverse cracks occur in a ply within the laminate, its mechanical properties are progressively degraded using a thermodynamic degradation approach based on continuum damage modelling. The initial elastic compliance is increased by the degradation of the failed ply in the in-plane interfibre mode. The kinetics of the degradation is distinguished from the effects of the transverse cracks. The effect tensor can be determined from knowledge of the elastic properties, while the calibration of the damage evolution law required one tensile test on a laminate. Finally, the 0-plies fail due to fibre failure which induces a violent and sudden drop load at the macroscopic scale. To describe that phenomenon, a softening failure behaviour has been proposed associated to a delay effect method to avoid mesh dependence problem. It must be noted that the fibre failure in tension is

distinguished to the fibre failure in compression (fibre kinking) since the physical mechanisms are completely different. To model delamination between plies with different orientations, Abaqus' built-in cohesive elements are considered. A classical quadratic stress criterion is considered for cohesive damage initiation, and the evolution of damage is controlled by the fracture energy. Mode-dependent damage evolution is also considered, by specifying the mode I and mode II interlaminar fracture toughness values. The BK law is considered to properly fit the mixed mode interlaminar fracture toughness evolution. It can be noted that, for now, the fracture toughness between the plies and the battery cells is considered similar which is an arguable assumption. More details on the failure model and its implementation in Abaqus/Explicit can be found in [6].

3.2. QUASI-STATIC SIMULATIONS

In the SOLIFLY project, a first composite plate with battery cells has been manufactured and tested considering AS4/8552 composite materials and the RMS battery cells.

3.2.1. Material properties (composite and cell part)

Table 1 shows the identified material parameters associated to the OPFM model using tests found in the literature [7,8] for the AS4/8552 unidirectional ply. Moreover, the properties associated to the delamination (onset and propagation) between plies are reported in **Fehler! Verweisquelle konnte nicht gefunden werden.**. It can be noted that the interface properties are considered similar for interfaces between plies and those between ply and battery cells.

***Table 1**. Properties of the AS4/8552 UD ply extracted from literature* [7,8]

Elasticity	
E_1^0	138000 MPa
E_2	10000 MPa
ν_{12}	0.3
ν_{23}	0.4
G_{12}	4900 MPa

Strength	
X^t	1950 MPa
X^c	-1100 MPa
Y^t	88 MPa
Y^c	-250 MPa
S_{12}^c	95 MPa
S_{23}^c	105 MPa

Elastic non-linearity in fibre direction		
In tension	$E_1^{t\infty}$	133000 MPa
	$\varepsilon_0^{t\infty}$	0.005
In compression	$E_1^{c\infty}$	132000 MPa
	$\varepsilon_0^{c\infty}$	0.012

Table 2. *Interface properties between AS4/8552 plies*

Fracture energy	
G_{IC}	0.30 N/mm
G_{IIC}	0.87 N/mm
η	1.45

Stiffness	
K_I	10^6 MPa
K_{II}	10^6 MPa
Strengths	
Z_t	74.2 MPa
S_c	110.4 MPa

During the SOLIFLY project, tensile tests with unloading have been performed on battery cells and have demonstrated that a plastic behaviour with an isotropic hardening [9] seems to be relevant to describe the measured behaviour.

a)

```
*Plastic, hardening=isotropic
12.1, 0.00
15.8, 0.10E-3
18.9, 0.25E-3
21.6, 0.41E-3
24.0, 0.63E-3
26.1, 0.88E-3
27.8, 1.16E-3
29.3, 1.48E-3
30.5, 1.81E-3
31.7, 2.17E-3
32.6, 2.56E-3
33.5, 2.92E-3
43.0, 10.13E-3
43.0, 16.00E-3
```

b)

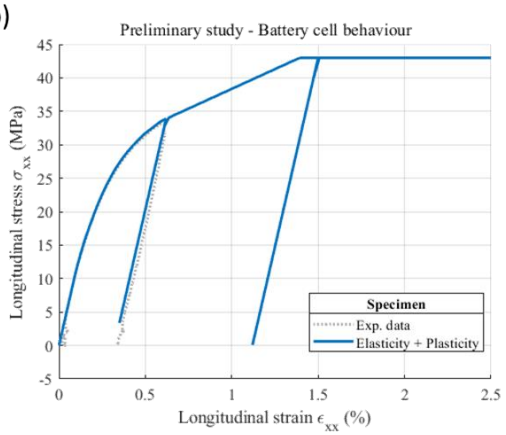

Figure 5: a) Identified true stress and strain, b) measured and simulated behaviour of RMS battery cells

Therefore, the available Abaqus plastic behaviour with an isotropic hardening has been considered. The identified true strain and stress points are reported in Figure 5a, and the comparison with experimental data, illustrated in Figure 5b, is in good agreement. It must be noted that the failure of the battery cells is not considered in the current version of the model.

3.2.2. First obtained results

The proposed modelling has been applied to a configuration that has been manufactured and tested in the SOLIFLY project. Therefore, as shown in Figure 4, two multi-electrode-layer battery cells have been integrated only in the central 90 plies and ±45 plies of a 16-ply quasi-isotropic $[(45/90/-45/0)_2]_s$ laminate, a lay-up which is widely used in the aeronautical industry. The battery cells have been integrated considering 2 blocks of 3 consecutive battery cells. The dimensions of the quasi-isotropic laminate, after machining with a water-cooled diamond saw, are 200 mm x 30 mm x 2.92 mm. The free length of the sample is 150 mm, with the remainder of the sample clamped in the hydraulic jaws. The in-plane size of the battery cells is 100 mm x 20 mm to obtain an in-plane section of approximately 2000 mm^2 for each battery cell.

Figure 6 presents the predicted macroscopic behaviour with OPFM model without battery cells in blue and it is compared with experimental data generated in the SOLIFLY project (blue dot line). Matrix cracking are predicted for a macroscopic strain equal to 0.75%, and finally fibre failure and delamination occur just prior the final failure at 1.4%. The predictions are in very good agreement with experimental data. Then, considering the battery cells included in the composite laminated plate, the predicted macroscopic modulus has been decreased about 3% considering an elastic behaviour for the battery cells and 4% considering the plastic behaviour (red line). The evolution of the onset of transverse cracks is not modified but it must be noted that the battery cells should fail for an applied macroscopic strain equal to 0.6% (leading to a decrease of the first damage event recorded during the test). Finally, the macroscopic stress at failure is decreased by 4% considering the elastic behaviour for the battery cells and 8% considering plasticity. The influence of the non linear behaviour of the battery cells is therefore non negligible on the quantity of interests.

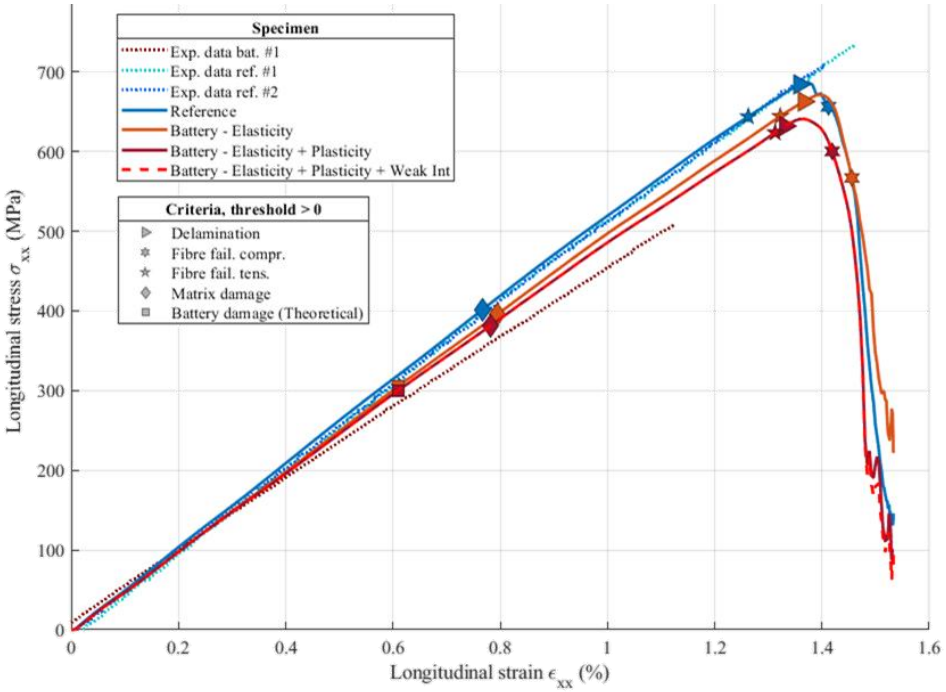

Figure 6: Predicted influence of the battery cells integration within a 16-plies quasi-isotropic laminate

It can be noted that the predictions tend to overestimate the experimental tests results (red dot line). It could be explained by several factors. Indeed, some initial out-of-plane ply waviness have been observed on the free edges of the specimens which has been polished, as illustrated in Figure 7. The external 45-ply located at the caul plate side seems to be pre-damaged. Moreover, some voids are observed mainly located at the interface between plies. The volume voids content is not negligible and measured optically (binarization of the image with a grey level threshold equal to 50 considering the 255 possible grey values) on a length of 80mm to c_p=2.5%. But it must be noted that the voids are only located in the 8 upper plies, meaning that the volume content is equal to 5% in those plies, which is non-negligible. Therefore, considering the model predictions, it seems that the decrease of the mechanical properties can be limited by improving the manufacturing process and thus the quality of the composite part around the battery cells.

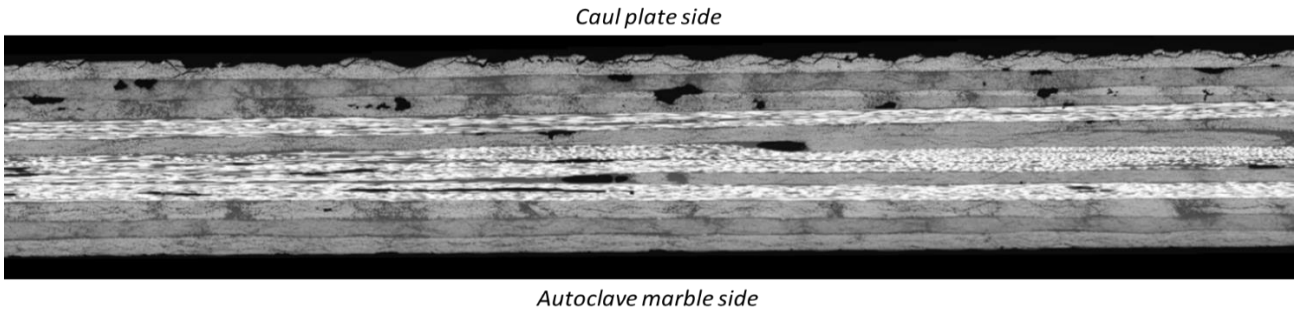

Figure 7: Analysis of one free polished edge of the composite plate with 6 embedded battery cells

The conclusions established here are applicable for tension loadings. Additional work needs to be carried out for bending loads which will be the loading applied to final demonstrator of the MATISSE project.

3.3. IMPACT SIMULATIONS

In order to study the dynamic response of a solid laminate with embedded battery cells, advanced models are developed in Abaqus explicit by Simulia. Using an explicit solver allows to evaluate the dynamic response of the component/specimen during the entire event with a reasonable computational cost and a good accuracy level.

The activities aim to evaluate the influence of the embedded batteries on the structural response of the laminate and the damage status due to an impact with respect to foreign objects.

This preliminary study was performed considering specimen according to the standard ASTM 7136, since no other specific standard were available.

A schematic picture of the test set-up (fixture and specimen) for the impact test is shown in Figure 8.

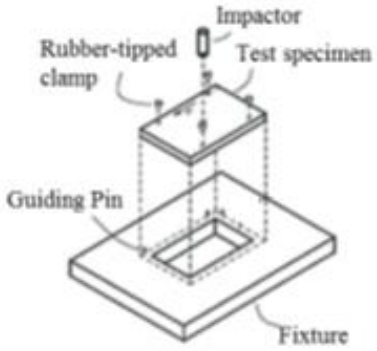

Figure 8: Test setup for impact test ASTM7136

The specimen consists of a rectangular and flat plate 100mm wide and 150 mm long. Generally, the specimen thickness depends on the impact energy threshold, but in such case, it is not relevant for our scope and it was fixed to 3.2mm (16 plies). The impact energy is about 46 J that corresponds to an impact velocity of 5m/s and an impact mass of 3.68kg.

In order to simulate the right boundary conditions, both supporting plate and the pins are modelled. The impactor is a hemispherical body with a diameter equal to 16mm.

The adopted staking sequence is [45, 90, -45, 0]2s – 16 plies and a battery cells of single ply thickness are placed in the plies oriented at 90°. Regarding the battery shape, both rectangular and elliptical ones were investigated.

The developed numerical models are shown in Figure 9-Figure 12. As already stated, the models include the supporting metallic plate (rigid body) and the pin used to keep in position the specimen during the impact, the impactor (rigid body) and the specimen.

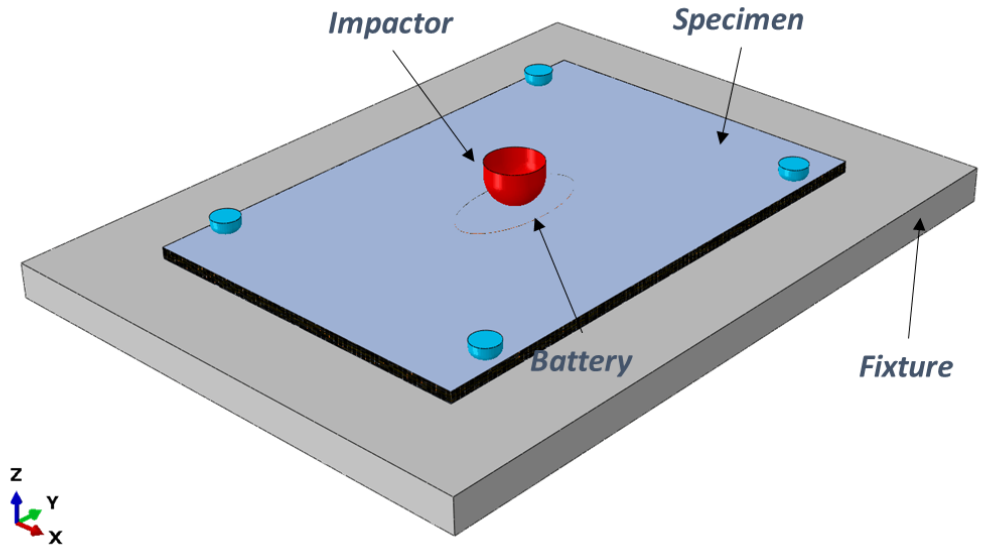

Figure 9: Numerical model of the composite specimen embedding battery cells subjected to impact test simulations

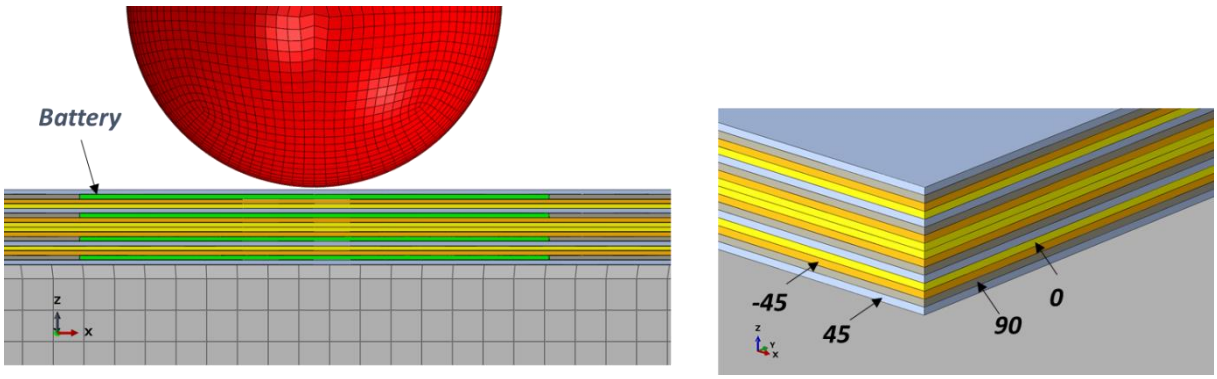

Figure 10: Stacking sequence and battery cells positions

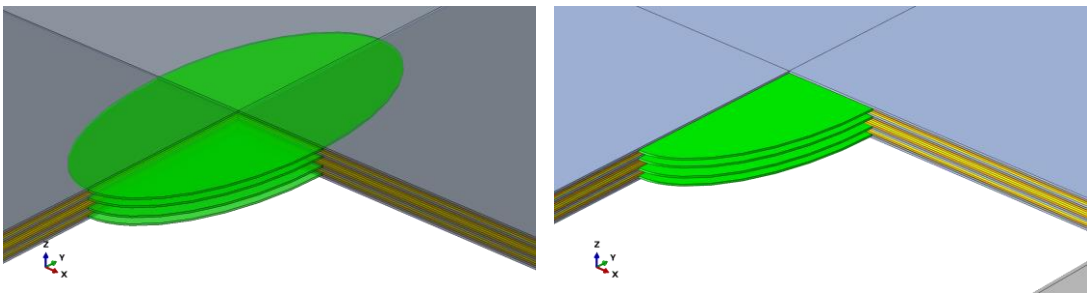

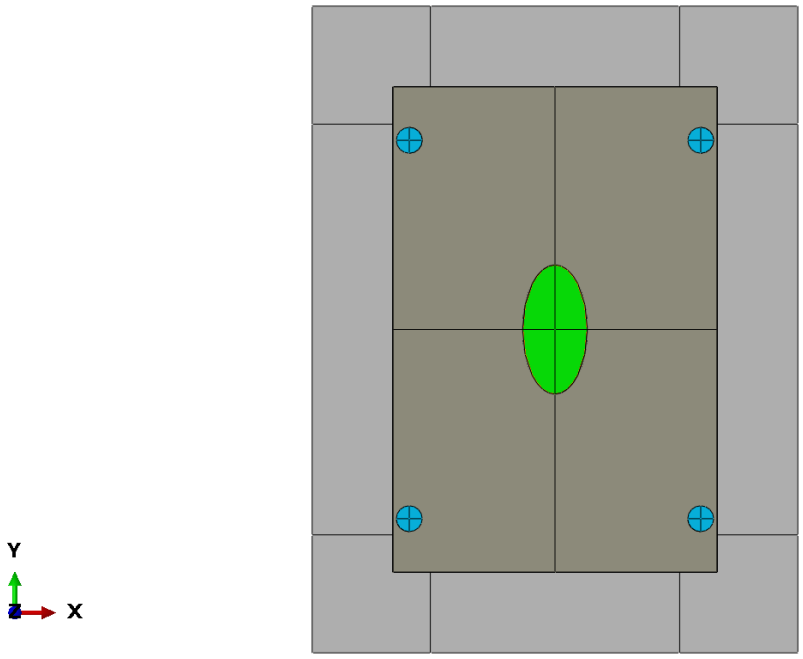

Figure 11: Details of the embedded battery cells with elliptical shape

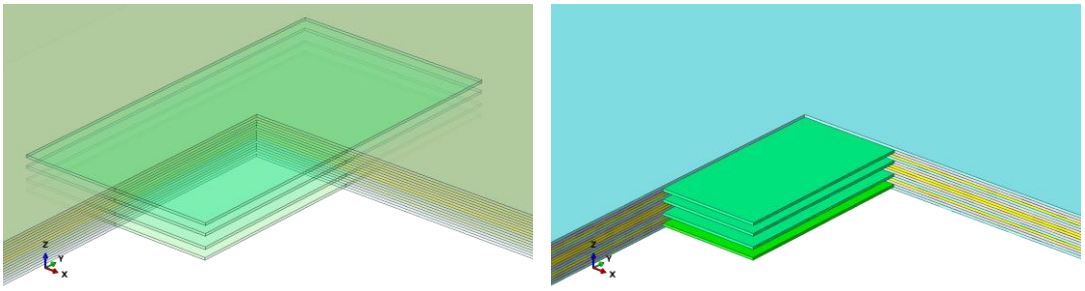

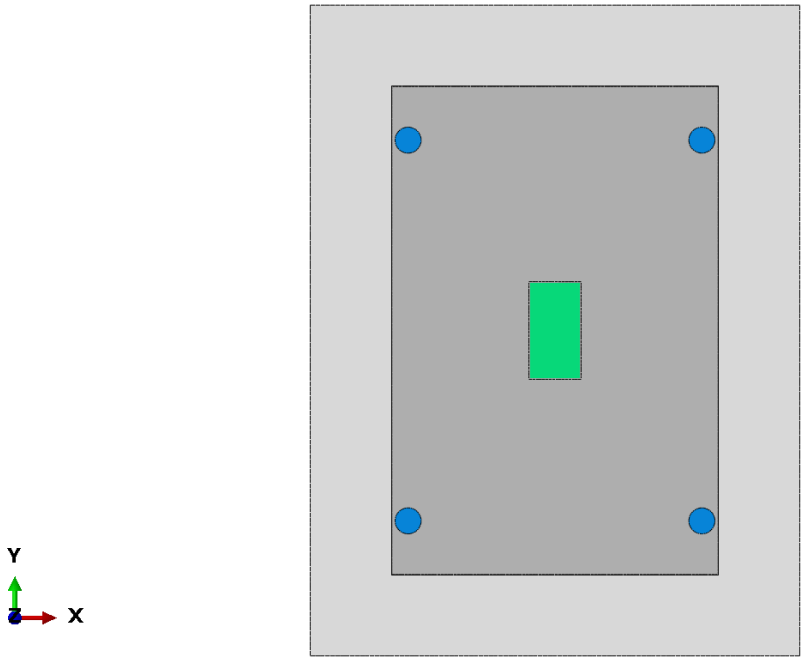

Figure 12: Details of the embedded battery cells with rectangular shape

A cohesive surface has been considered between the batteries and the plies in order to simulate the debonding onset and propagation. Similar interactions have been defined between the other adjacent plies. The material model adopted includes per progressive failure option at lamina level.

Two different cohesive set data have been considered in order to estimate a possible dependency by such parameters. The two sets data are reported in Table 3 and referred to as C-set A and C-set B. The C-set A correspond to typical values for CFPR materials which are used to simulate the delamination onset and propagation. For both set the cohesive stiffens are in the order of 10e+6 MPa.

Table 3: Cohesive properties of the surface between the plies and the batteries

Cohesive Property	C-set A	C-set B
N_{max} (normal direction) [N]	25	75
S_{max} (first shear direction) [N]	100	200
T_{max} (second shear direction) [N]	100	200
GI_c (fracture toughness Mode I)	0.3	0.6
GII_c (fracture toughness Mode II)	0.6	1.2
$GIII_c$ (fracture toughness Mode III)	0.6	1.2

Figures 13-20 report a comparison between the two cohesive material data regarding the case with elliptical battery cells in terms of global displacement and deformed shape in section view.

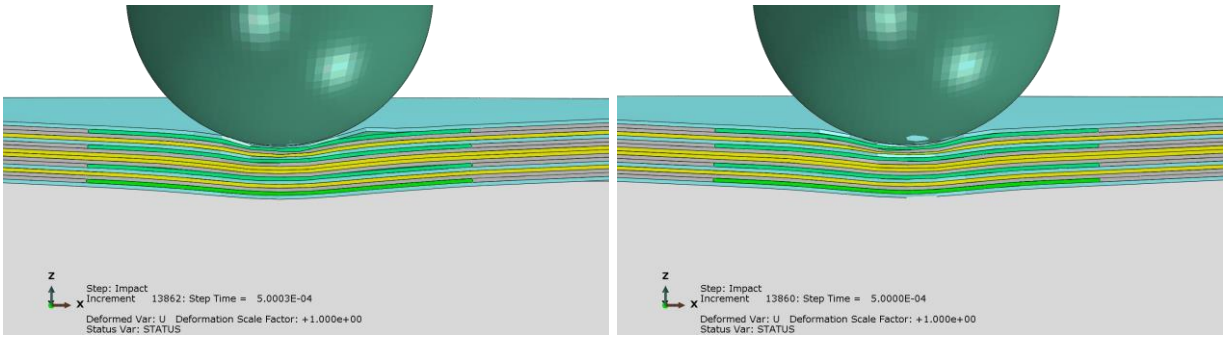

Figure 13: Elliptical shape - global displacement @ 0.5 ms – left: C-Set A; right: C-Set B

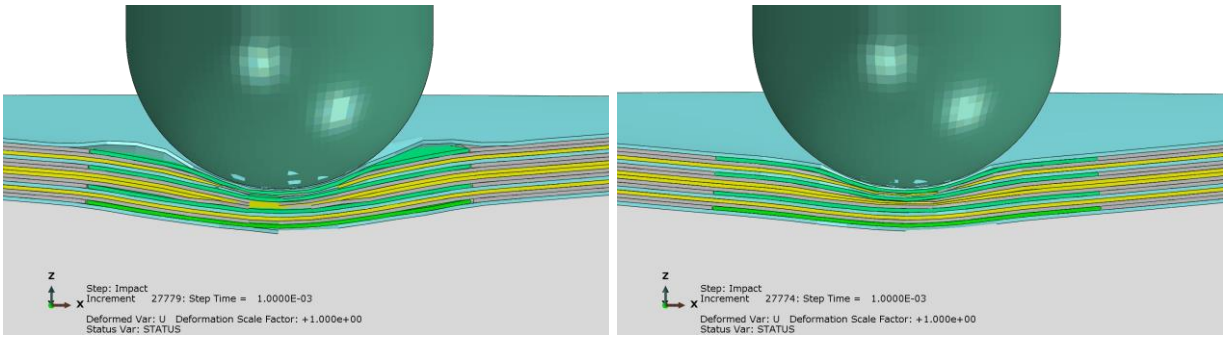

Figure 14: Elliptical shape - global displacement @ 1.0 ms – left: C-Set A; right: C-Set B

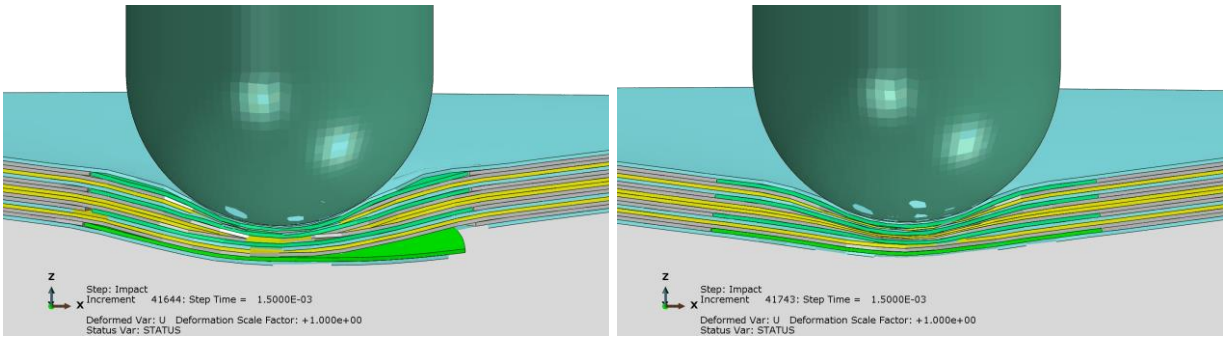

Figure 15: Elliptical shape - global displacement @ 1.5 ms – left: C-Set A; right: C-Set B

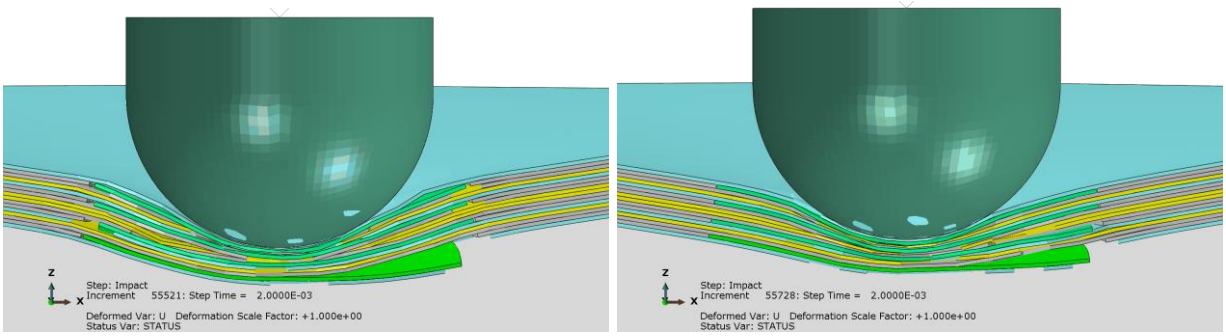

Figure 16: Elliptical shape - global displacement @ 2.0 ms – left: C-Set A; right: C-Set B

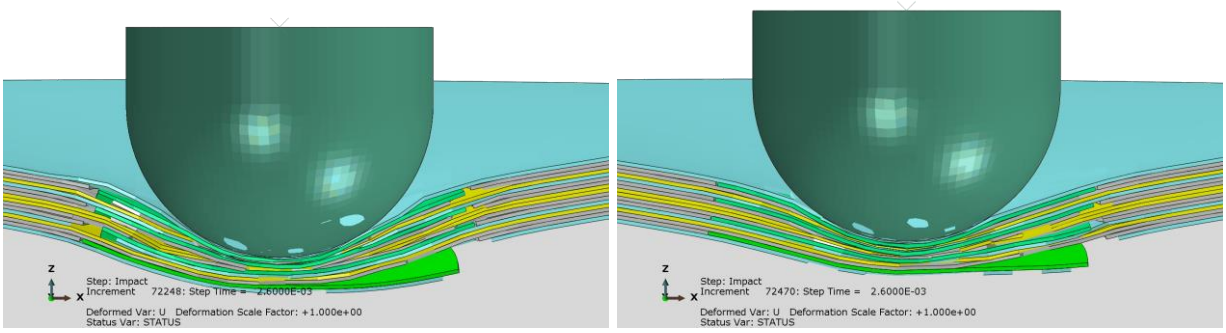

Figure 17: Elliptical shape - global displacement @ 2.6 ms – left: C-Set A; right: C-Set B

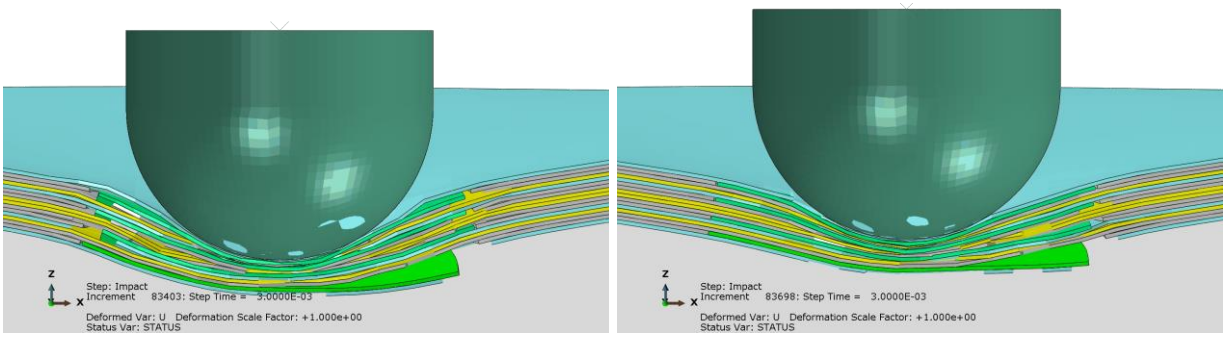

Figure 18: Elliptical shape - global displacement @ 3.0 ms – left: C-Set A; right: C-Set B

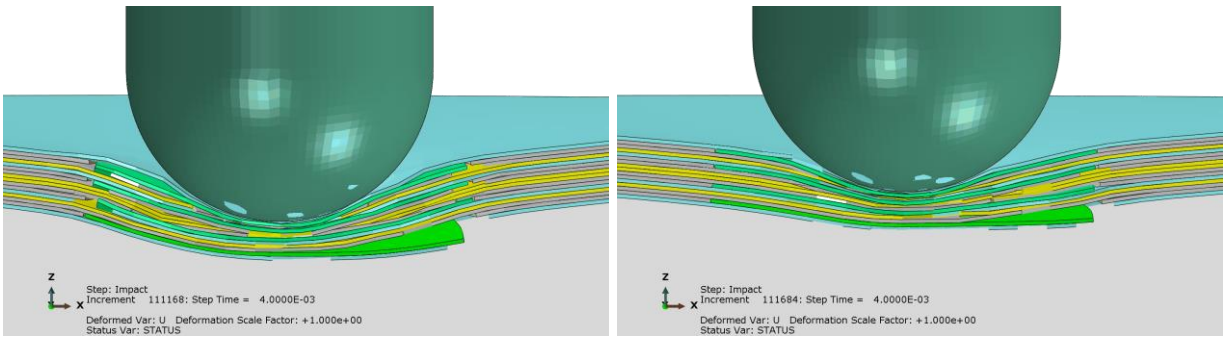

Figure 19: Elliptical shape - global displacement @ 3.5 ms – left: C-Set A; right: C-Set B

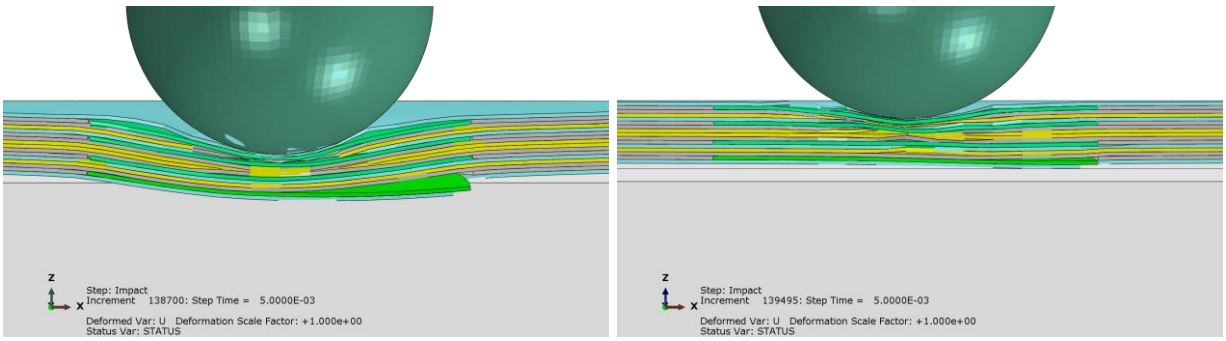

Figure 20: Elliptical shape - global displacement @ 5.0 ms – left: C-Set A; right: C-Set B

In order to better understand the structural response, the energy balances are reported in Figure 21 and Figure 22 for both materials set data. In case B the damage energy has a rapid growth and the strain energy has a clearer fall at about 1.5 ms. Such a behaviour can be related to a quick damage onset and propagation in the batteries' interfaces and to a more extended damage status.

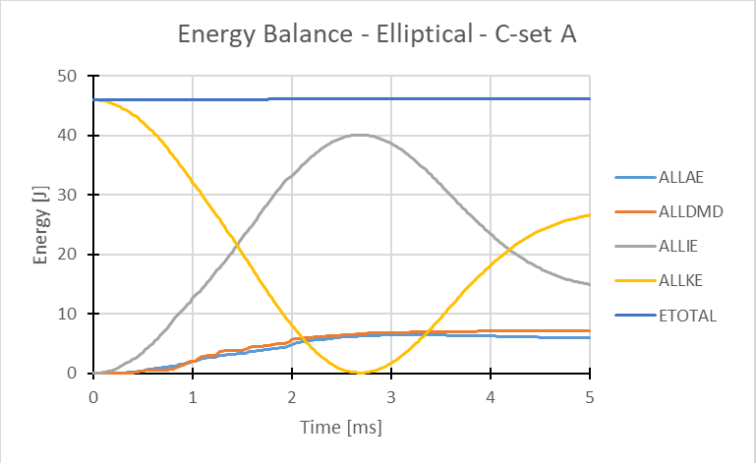

Figure 21: Energy balance - Elliptical shape - cohesive material set A

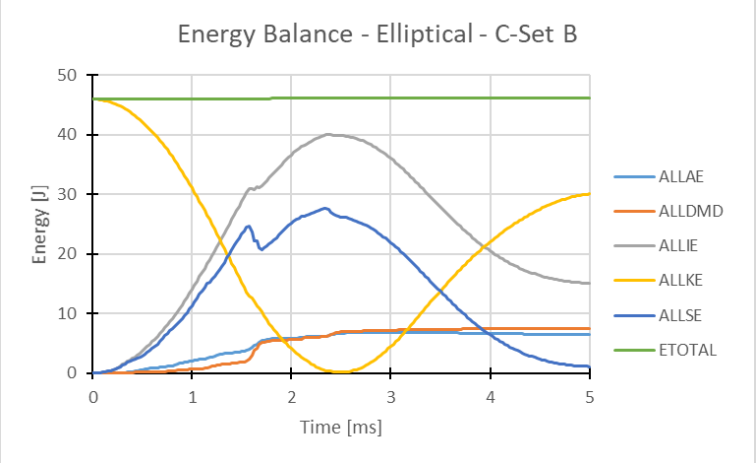

Figure 22: Energy balance - Elliptical shape - cohesive material set B

The bigger damage status can be detected also in the impactor displacement time history (along impact direction), reported in Figure 23.

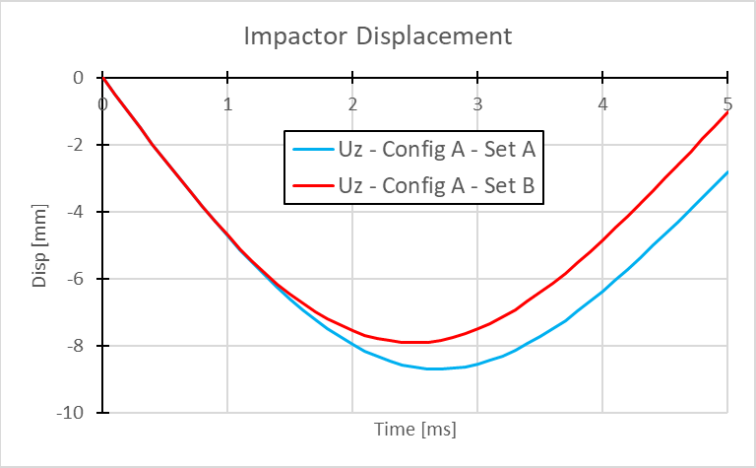

Figure 23: Impactor displacement time-history – Elliptical shape - Comparison between C-Set A and B

It is worth noting that using smaller cohesive properties leads to bigger damage status and a premature loss in stiffness that is translated in bigger impactor displacement and in a slower go back.

Similar consideration can be done by analysing the kinetic energy time history, reported in Figure 24.

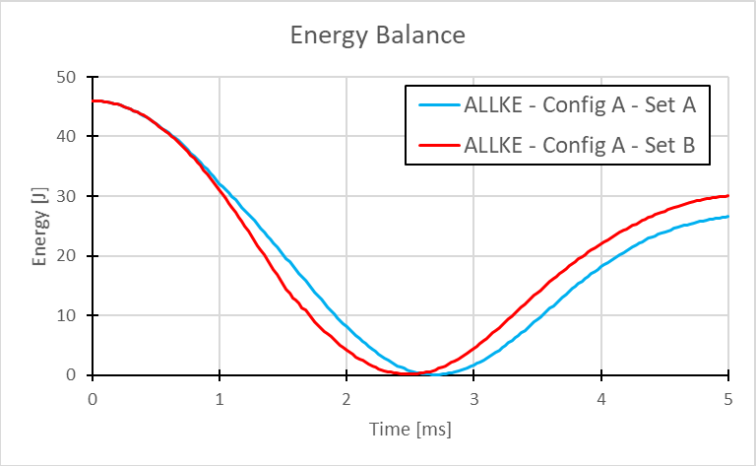

Figure 24: Kinetic energy time-history – Elliptical shape - Comparison between C-Set A and B

An equivalent investigation was performed considering the battery cells with rectangular shape. Figures 25 to 32 report a comparison between the two cohesive material data regarding the case with rectangular battery cells in terms of global displacement and deformed shape in section view.

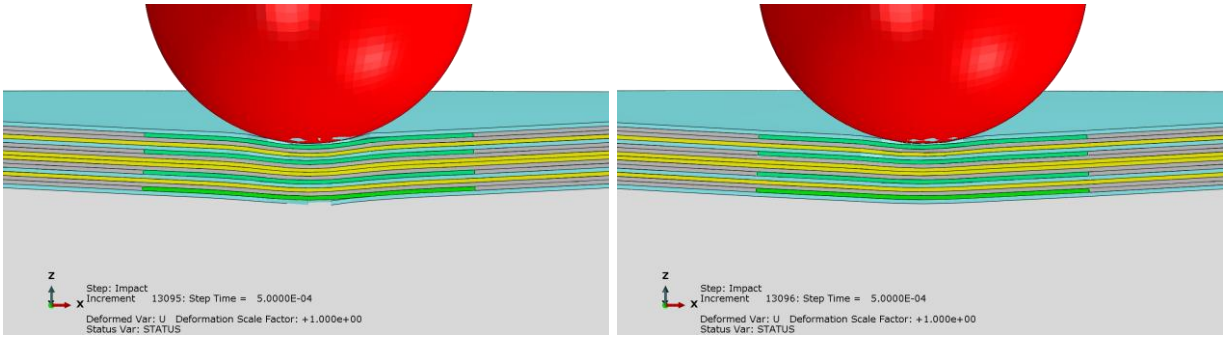

Figure 25: Rectangular shape - global displacement @ 0.5 ms – left: C-Set A; right: C-Set B

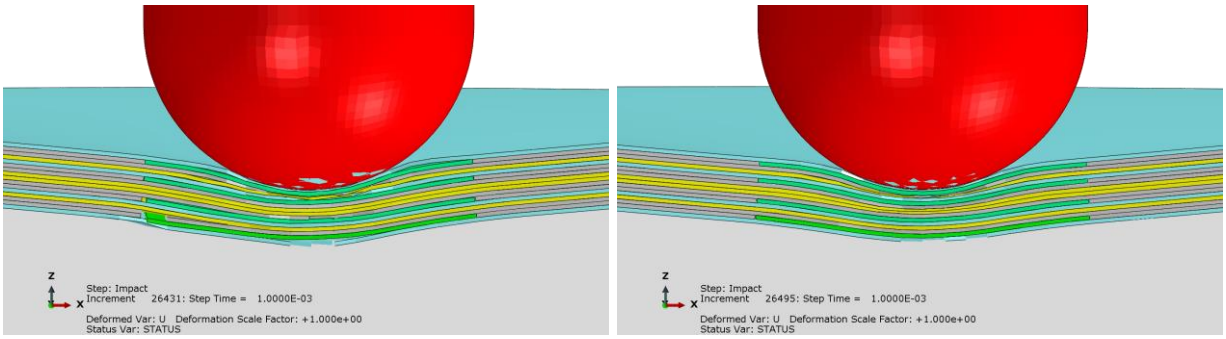

Figure 26: Rectangular shape - global displacement @ 1.0 ms – left: C-Set A; right: C-Set B

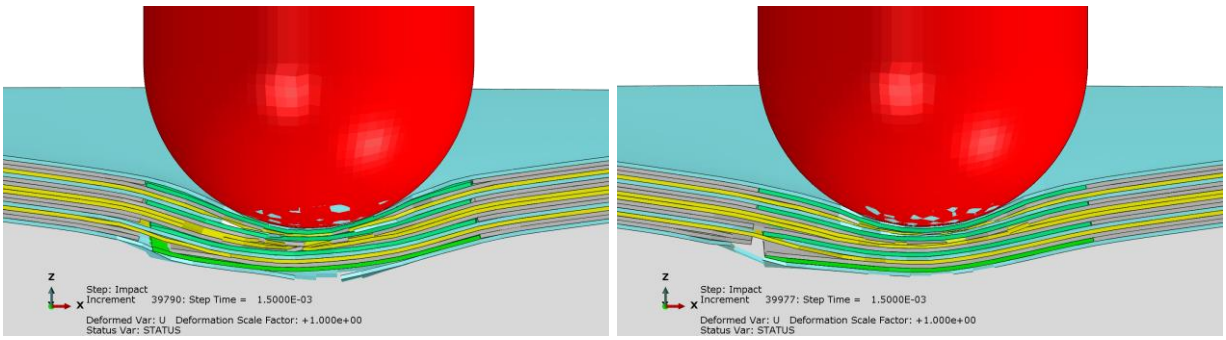

Figure 27: Rectangular shape - global displacement @ 1.5 ms – left: C-Set A; right: C-Set B

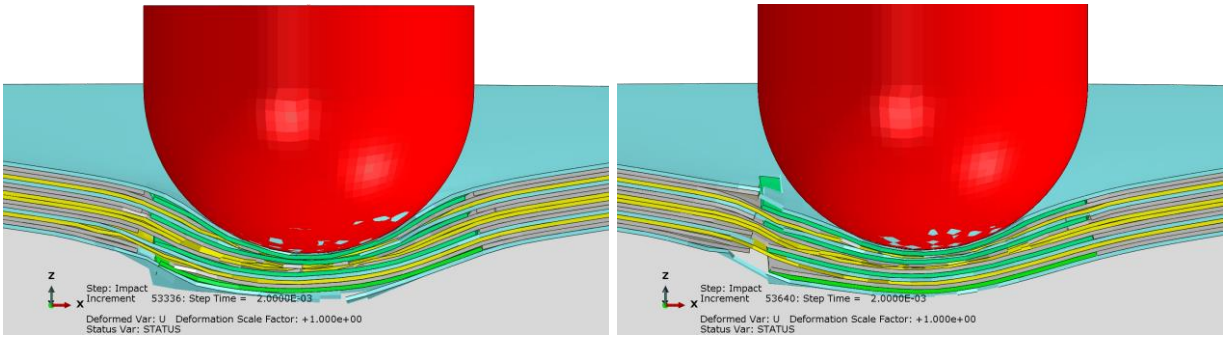

Figure 28: Rectangular shape - global displacement @ 2.0 ms – left: C-Set A; right: C-Set B

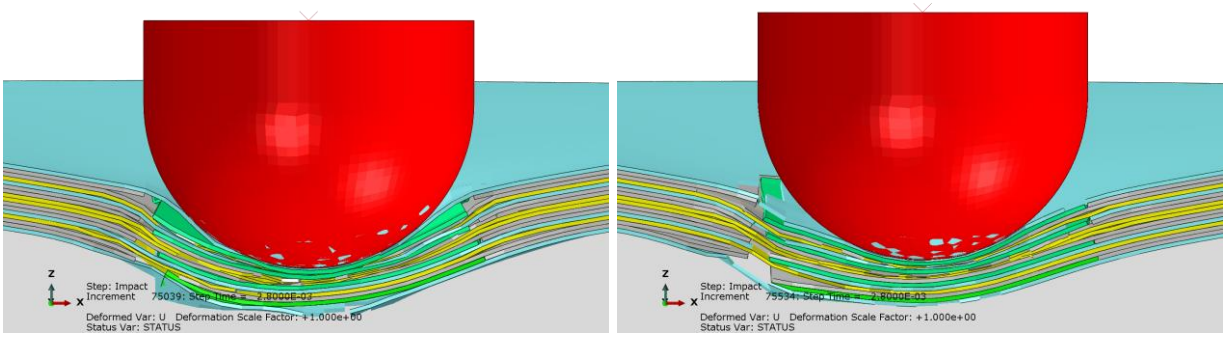

Figure 29: Rectangular shape - global displacement @ 2.8 ms – left: C-Set A; right: C-Set B

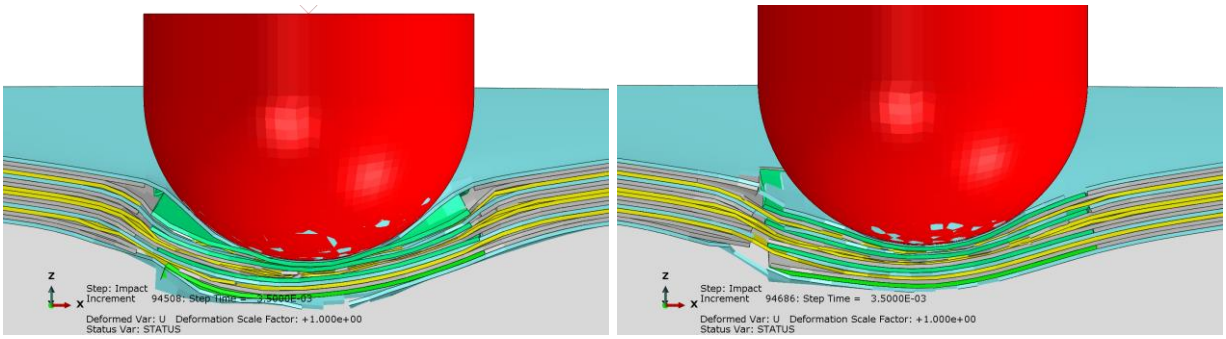

Figure 30: Rectangular shape - global displacement @ 3.5 ms – left: C-Set A; right: C-Set B

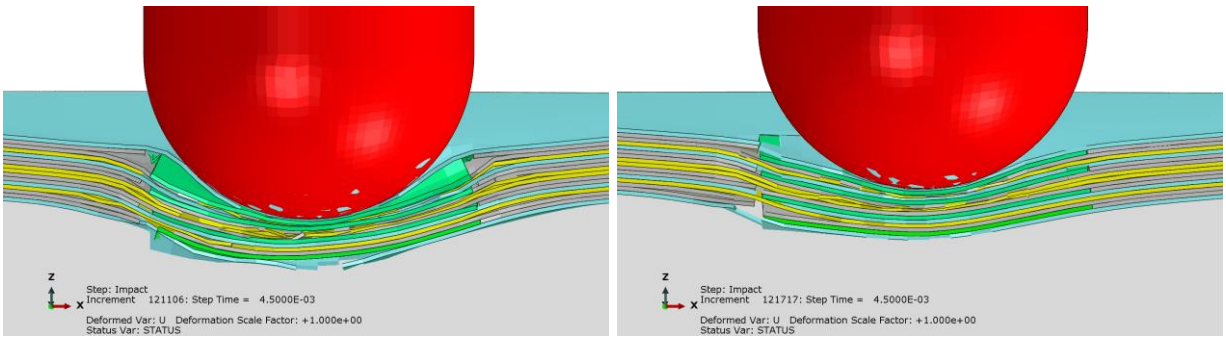

Figure 31: Rectangular shape - global displacement @ 4.5 ms – left: C-Set A; right: C-Set B

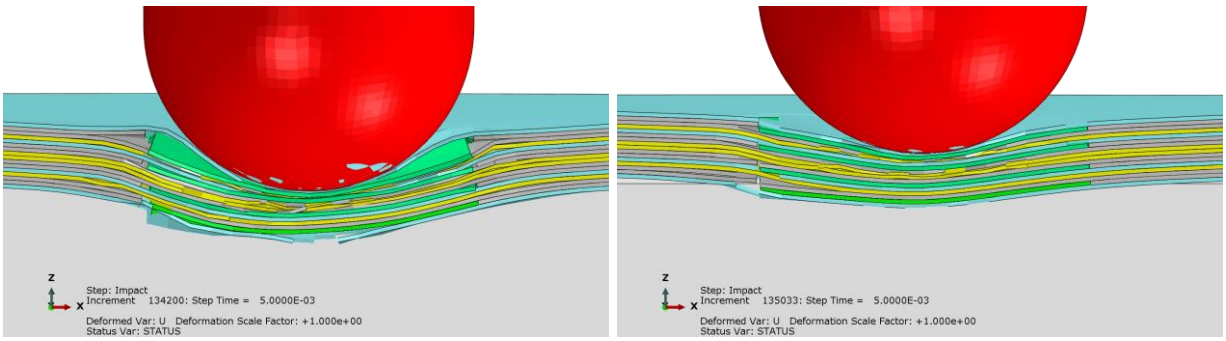

Figure 32: Rectangular shape - global displacement @ 5.0 ms – left: C-Set A; right: C-Set B

The energy balances are reported in Figure 33 and Figure 34 for both materials set data. In case B the damage energy has a rapid growth and the strain energy has a clearer fall at about 1.5 ms. Such behaviour can be related to a quick damage onset and propagation in the batteries' interfaces and to a more extended damage status.

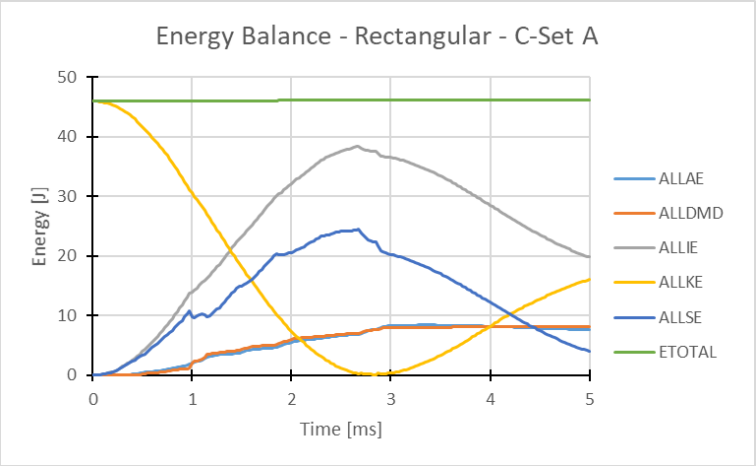

Figure 33: Energy balance - rectangular shape - cohesive material set A

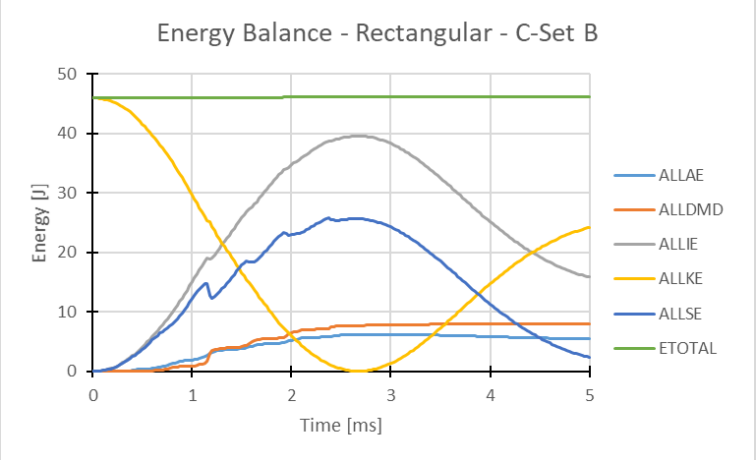

Figure 34: Energy balance – Rectangular shape - cohesive material set B

The bigger damage status is confirmed by the impactor displacement time history (along impact direction), reported in Figure 35.

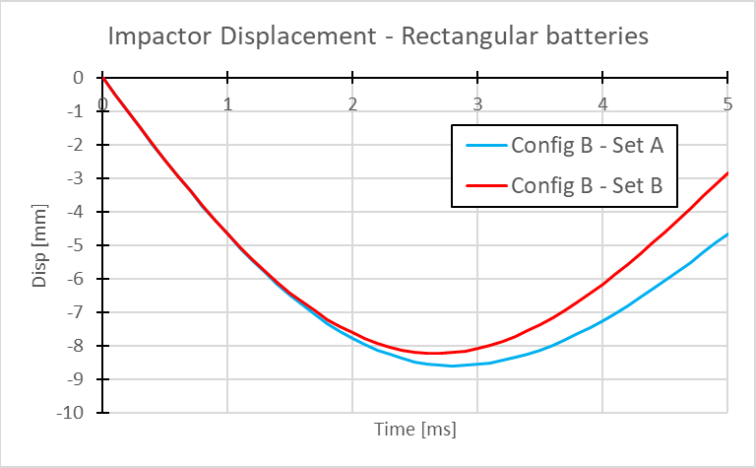

Figure 35: Impactor displacement time-history – Rectangular shape - Comparison between C-Set A and B

Smaller cohesive properties lead to bigger damage status and a premature loss in stiffness. Similar consideration can be done analysing the kinetic energy time history, reported in Figure 36.

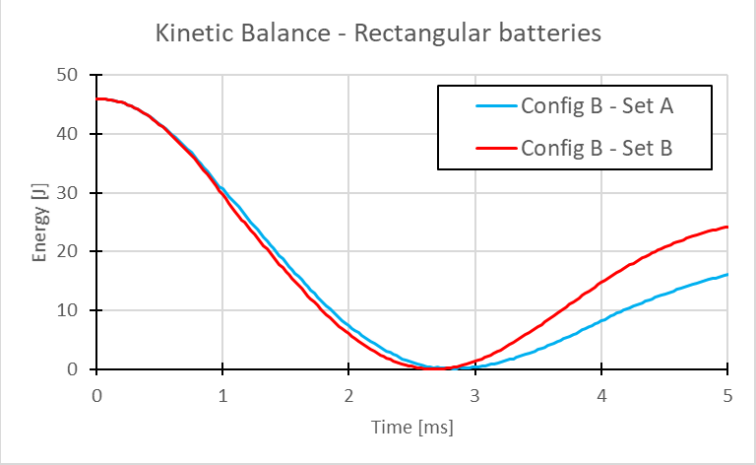

Figure 36: Kinetic energy time-history – Rectangular shape - Comparison between C-Set A and B

A comparison between of the impactor displacement curves for elliptical and rectangular cells is shown in Figure 37 and Figure 38, for both materials set A and set B respectively. These curves confirm that the elliptical shape has to be preferred with respect to the rectangular one, independently by the cohesive material data. Obviously, a deeper evaluation should be done by considering more realistic material data in terms of fracture toughness at battery-composite interface level.

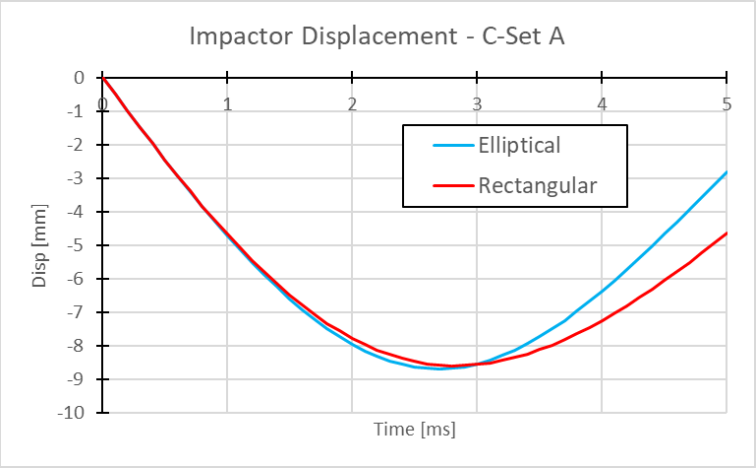

Figure 37: Comparison between elliptical and rectangular cells considering material set A

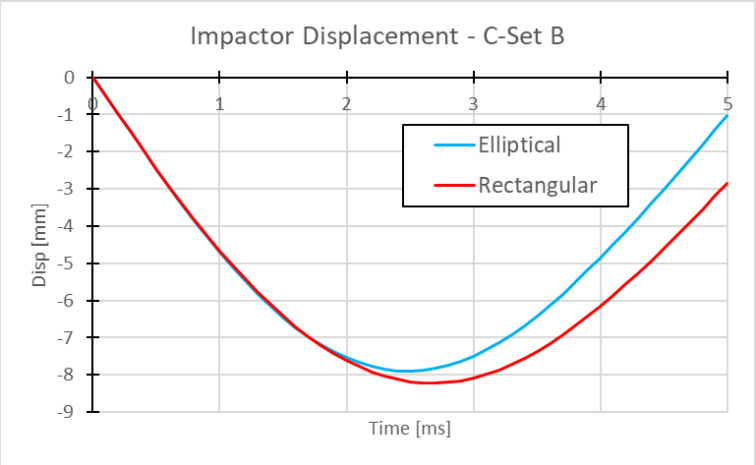

Figure 38: Comparison between elliptical and rectangular cells considering material set B

4. STRUCTURAL INTEGRATION CONCEPTS – SANDWICH LAMINATES

4.1. DESIGN METHODOLOGY

In order to determine the best configuration for embedding battery cells inside sandwich structures, an automatic FE modelling procedure was developed to predict the resulting mechanical performance of the multifunctional assembly. The procedure is currently still under development in order to refine and expand its capabilities. The routine was developed in the ANSYS environment and is based on an APDL script that allows to generate automatically different types of structures and insert the batteries trough the thickness choosing the shape, the number, the dimensions and relative position.

The routine is designed to create both solid laminate and sandwich structures and therefore, based on such a choice, several options for inserting the batteries are available. For example, as regards the sandwich structures, it is possible to insert the batteries both in the faces and in the core.

The numerical model is generated using 3D-solid elements in order to be able to correctly discretize the interaction between batteries and structure. These interfaces are modelled with cohesive surfaces that allow to simulate both the damage onset and propagation at a lower computational cost compared to modelling cohesive elements. At this stage of the project, the routine allows to create simple structures (plates) embedding the battery cells. However, it will be enhanced by adding further functionalities, such as importing geometric models and positioning the batteries directly on them. In this perspective, hybrid shell-solid modelling will also be carried out. The shell modelling will be applied in areas away from the batteries and where the thicknesses are compatible with such discretization approach.

Additionally, the APDL routine allows to automatically perform specific analyses and enables automated post-process procedures (the detail level of the post-processing is completely customizable). The ANSYS solver is used for quasi-static simulations, both linear and nonlinear (implicit solver). In order to allow the simulation in an explicit dynamic environment, the routine automatically converts the models from ANSYS to Abaqus. Of course, after importing the model into Abaqus, it can be used for implicit simulations too. Since the dynamic simulations are quite expensive, from a computational point of view, they are less suitable for an optimization analysis; therefore, in the definition phase, the ANSYS software was preferred as model generator.

The workflow shown in Figure 39 schematically illustrates the phases of the design process.

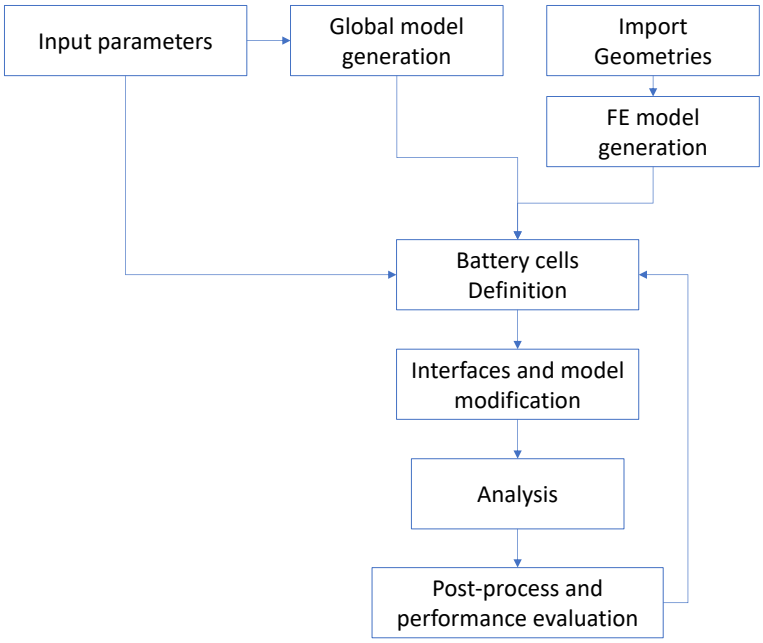

Figure 39: Workflow of the developed integration concepts design procedure

The model can be used in a stand-alone mode or in an integrated mode with a specific optimization tool. In the stand-alone mode the script allows to reduce the time need to generate the model and perform the post-process. It can be used also in a sort of loop in order to analyse automatically a specific set of design parameters.

A set of possible models that can be obtained using the developed design procedure are reported in Figure 40.

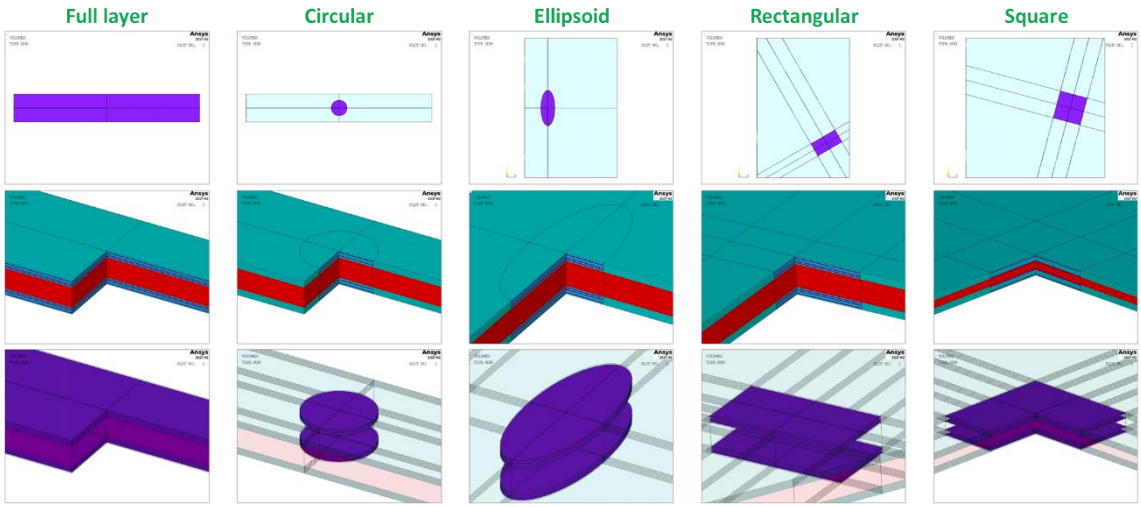

Figure 40: FE models generated by the automated structural batteries design and simulation procedure

If a specific optimization tool is used, the routine represents the core of the optimization procedure. The optimization process is performed by means of the Modefrontier software, which is highly versatile and allows for the use of a large number of optimization algorithms. Due to the nature of the problem, the most suitable software could be the MOGA-II which is a multi-objective genetic algorithm. In that procedure, Modefrontier calls ANSYS on-demand to generate the specific model based on the design variables according to the selected optimization scheme.

A typical Modefrontier workflow is reported in Figure 41. The main nodes are present: design variables; constraint functions, objective functions, optimization algorithm; starting population generator and analysis nodes (ANSYS).

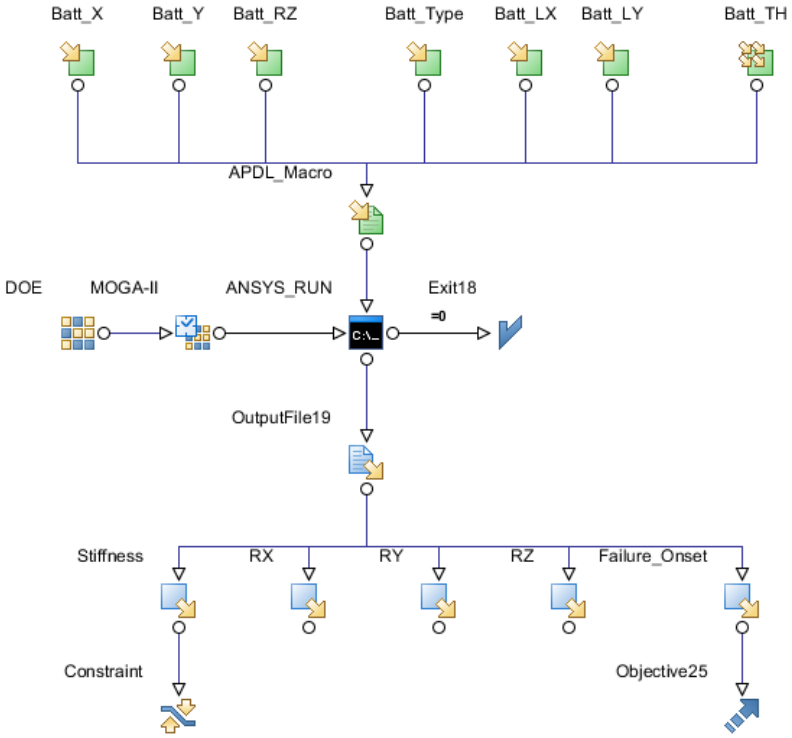

Figure 41: Typical Modefrontier workflow

4.2. IMPACT SIMULATIONS

The evaluation of the mechanical response under dynamic load condition of sandwich plates has been performed using the same approach adopted to study the solid laminate response. Dedicate numerical models have been defined, and, in particular, the software adopted to perform such activities is Abaqus explicit by Simulia. Using an explicit solver allows to evaluate the dynamic response of the component/specimen during the entire event with a reasonable computational cost and a good accuracy level.

The activities aim to evaluate the influence of the embedded batteries on the structural response of the sandwich plate and the damage status due to an impact with respect to foreign objects.

This preliminary study has been performed considering specimen defined in according to the standard ASTM 7136, since no other specific standard are available at the moment.

The specimen consists in a rectangular and flat plate 100mm wide and 150 mm long. Generally, the specimen thickness depends by the impact energy threshold, but in such case, it is not relevant for our scope and it was fixed to 8.2mm. The core thickness is 5 mm and each face is 1.6mm thick (8 plies).

The impact energy is about 46 J that corresponds to an impact velocity of 5m/s and an impact mass of 3.68kg.

In order to simulate the right boundary conditions both supporting plate and the pins have been modelled. The impactor is a hemispherical body with a diameter equal to 16mm.

The adopted staking sequence for each face is [45, 90, -45, 0]s – 8 plies and the battery cells have been placed in the core. Regarding the battery shape, since the previous study performed on the solid laminate has highlighted that the elliptical shape generates a reduced damage status, only the elliptical one has been considered to be integrated in the sandwich plate. The core was supposed made in foam and in particular the mechanical properties of the Rohacell 300WF have been considered, and its total thickness is 5mm.

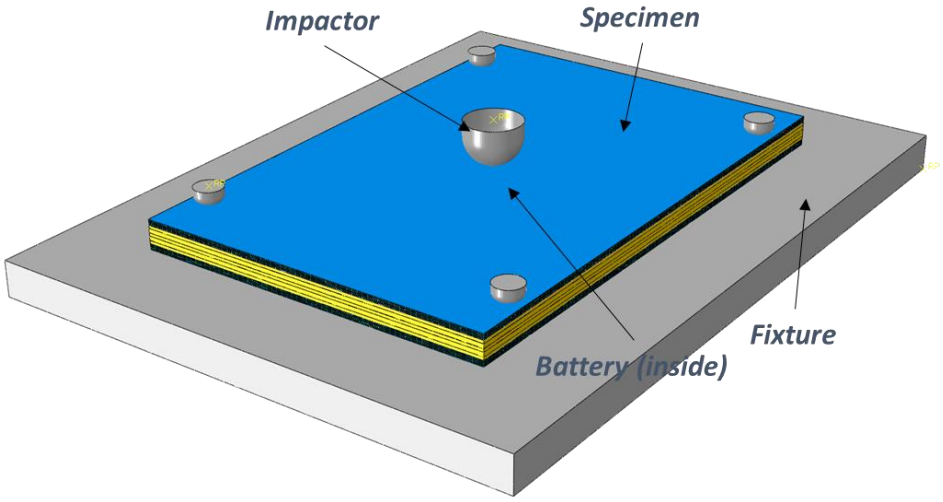

Figure 42: Numerical model of the sandwich laminate embedding battery cells subjected to impact test simulations

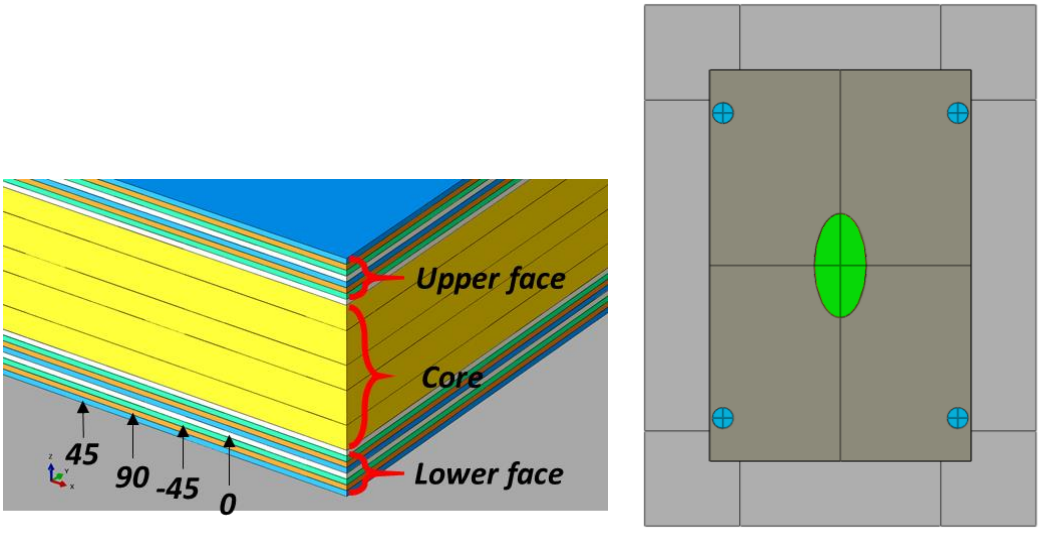

Figure 43: Model details. Left: stacking sequence; Right: battery shape and location

The battery cells are placed in the core thickness and two different configurations were analysed: 1 battery and 2 batteries. Each battery is made by 6 cells and its total thickness is 1.2 mm. The two configurations are referred to as Config A (1 battery) and Config B (2 batteries).

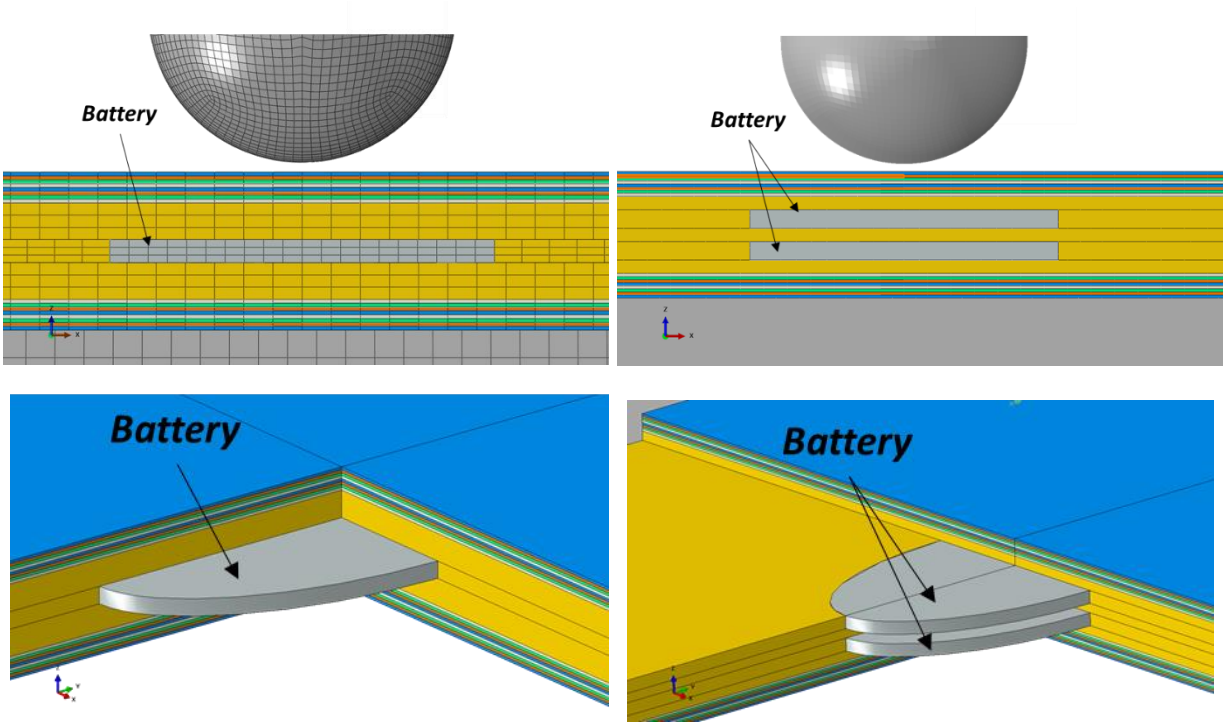

Figure 44: Details of the embedded battery cells with elliptical shape; Left: Config A; Right: Config B

Between the batteries and the neighbouring plies a cohesive surface was considered in order to simulate the debonding onset and propagation. Similar interactions were defined between the other adjacent plies, between plies and core and between the core layers (it was considered sliced for battery installation). The material model adopted includes per progressive failure option at lamina level.

Regarding the cohesive properties of the interaction battery-core the C-set B (used in the solid laminate study) was used. The cohesive properties are listed in Table 4.

Table 4: Cohesive properties (C-set B) simulating the interaction between SB cell and sandwich core

Cohesive Property	C-set B
N_{max} (normal direction) [N]	75
S_{max} (first shear direction) [N]	200
T_{max} (second shear direction) [N]	200
GI_c (fracture toughness Mode I)	0.6
GII_c (fracture toughness Mode II)	1.2
$GIII_c$ (fracture toughness Mode III)	1.2

The C-set A (defined in section 4), representative of typical values for CFPR materials, was used to model the remaining interactions. For both sets the cohesive stiffens is on the order of 10e+6 MPa.

Figures 45-57 report a comparison between the two analysed battery configurations considering an elliptical battery shape in terms of global displacements and deformed shape in a section view (central section).

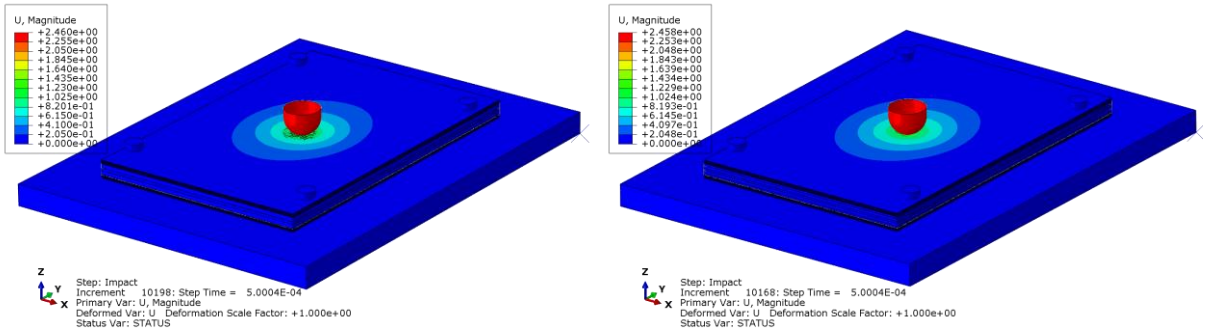

Figure 45: Elliptical shape – global displacement @ 0.5 ms – left:1 battery; right: 2 batteries

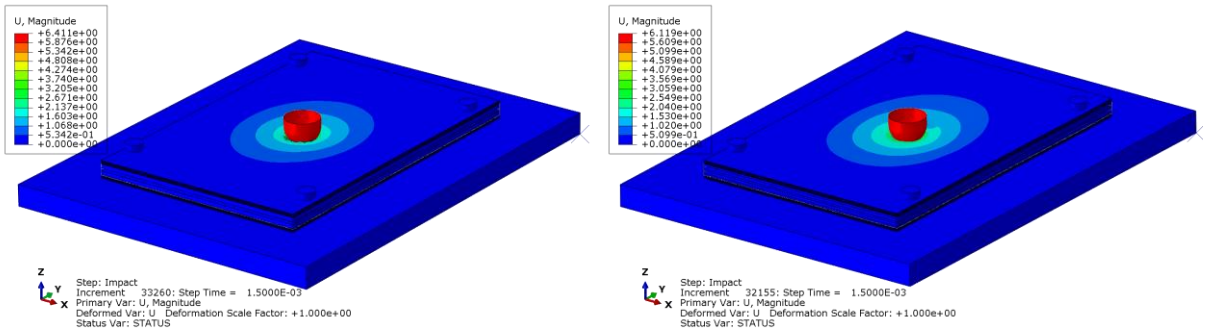

Figure 46: Elliptical shape – global displacement @ 1.5 ms – left:1 battery; right: 2 batteries

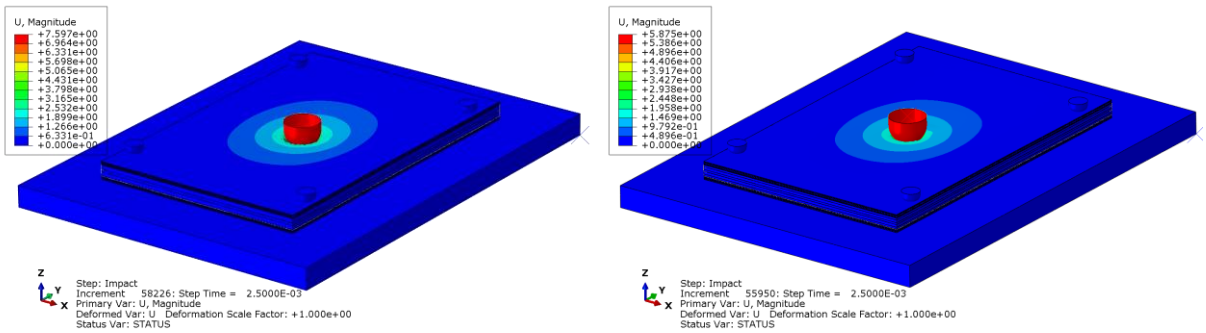

Figure 47: Elliptical shape – global displacement @ 2.5 ms – left:1 battery; right: 2 batteries

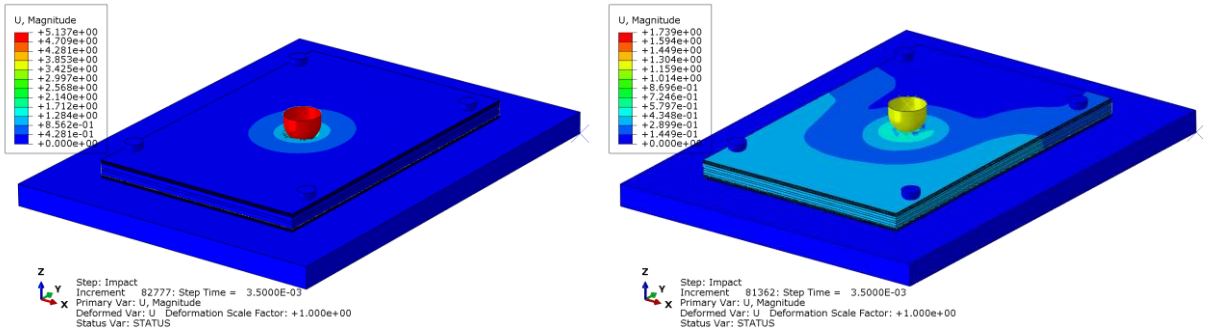

Figure 48: Elliptical shape – global displacement @ 3.5 ms – left:1 battery; right: 2 batteries

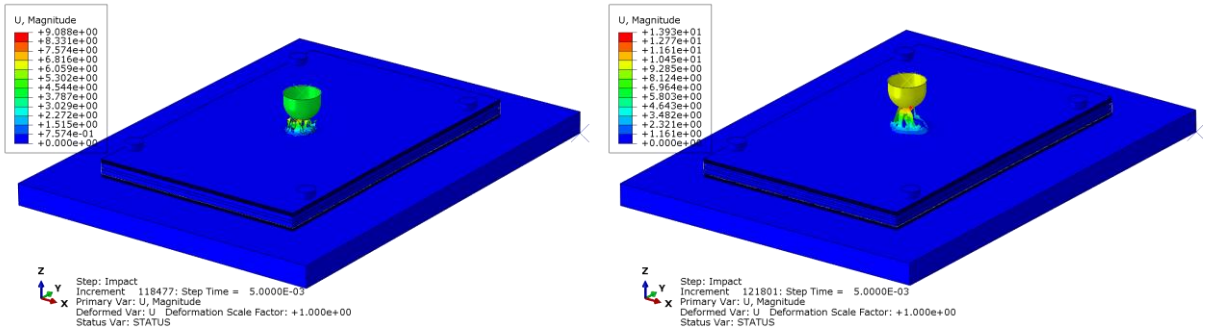

Figure 49: Elliptical shape – global displacement @ 5.0 ms – left:1 battery; right: 2 batteries

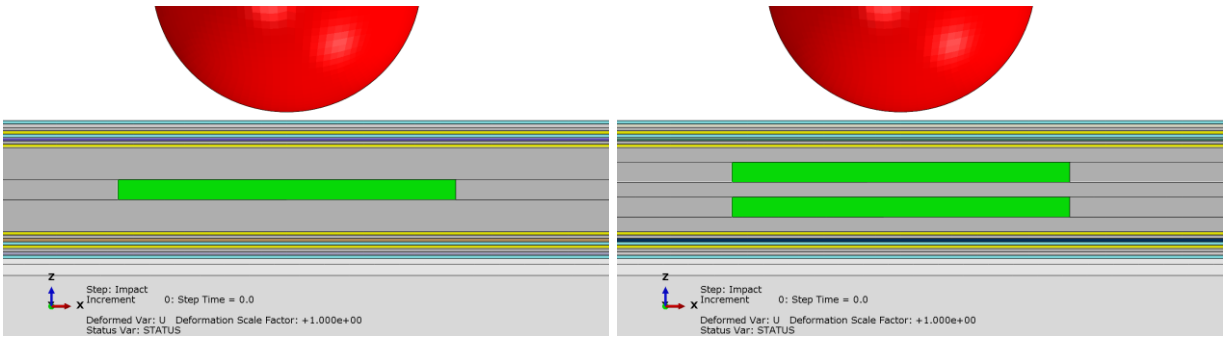

Figure 50: Elliptical shape – deformed shape in central section @ 0.0 ms – left:1 battery; right: 2 batteries

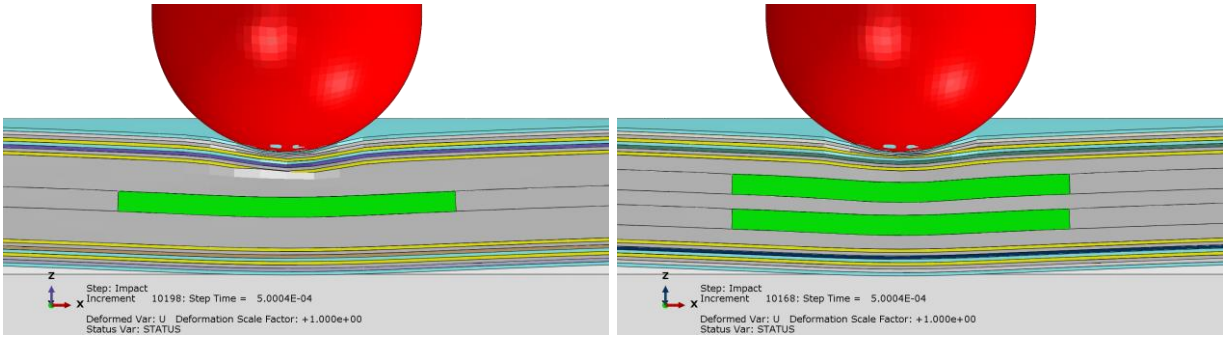

Figure 51: Elliptical shape – deformed shape in central section @ 0.5 ms – left:1 battery; right: 2 batteries

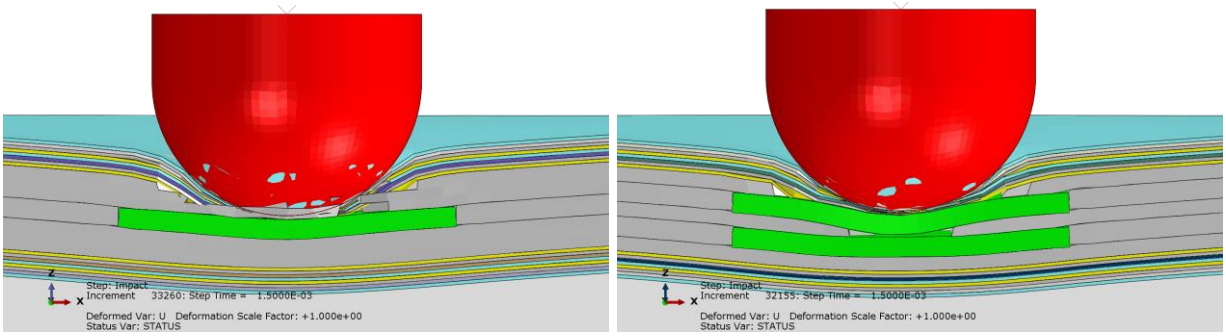

Figure 52: Elliptical shape – deformed shape in central section @ 1.5 ms – left:1 battery; right: 2 batteries

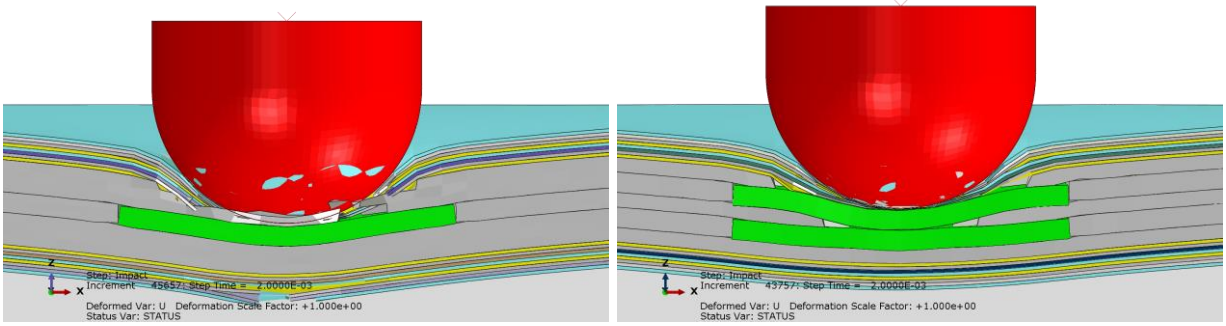

Figure 53: Elliptical shape – deformed shape in central section @ 2.0 ms – left:1 battery; right: 2 batteries

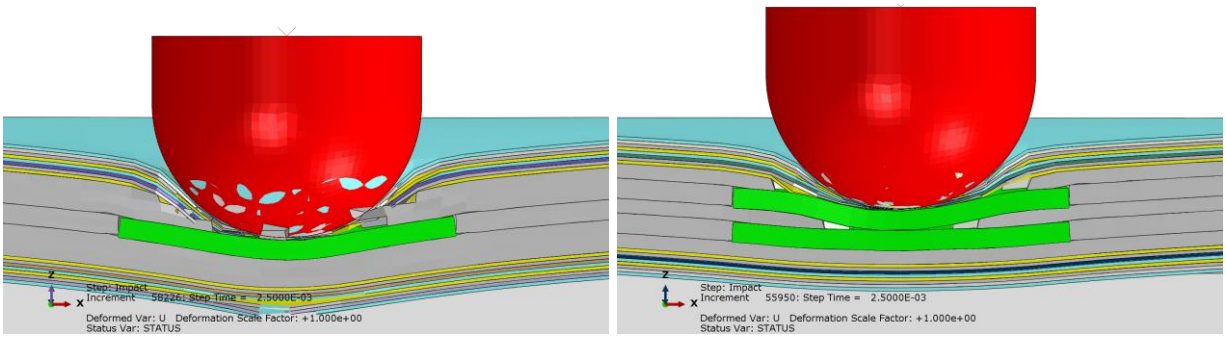

Figure 54: Elliptical shape – deformed shape in central section @ 2.5 ms – left:1 battery; right: 2 batteries

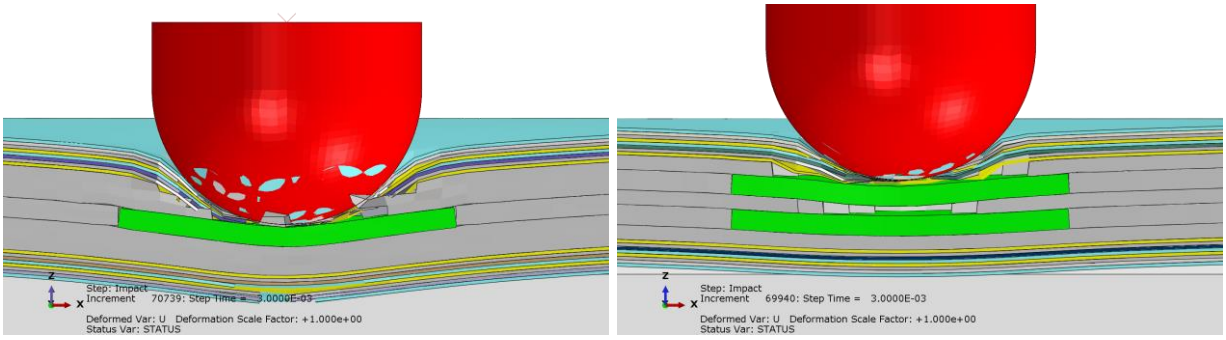

Figure 55: Elliptical shape – deformed shape in central section @ 3.0 ms – left:1 battery; right: 2 batteries

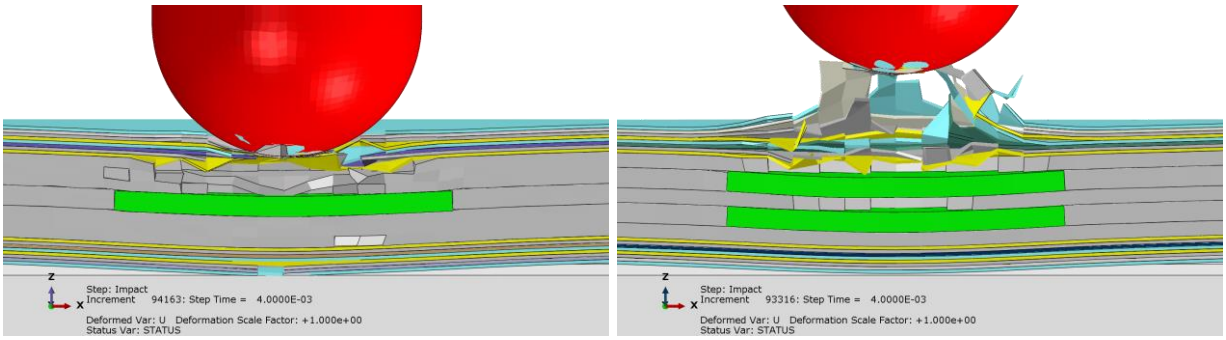

Figure 56: Elliptical shape – deformed shape in central section @ 4.0 ms – left:1 battery; right: 2 batteries

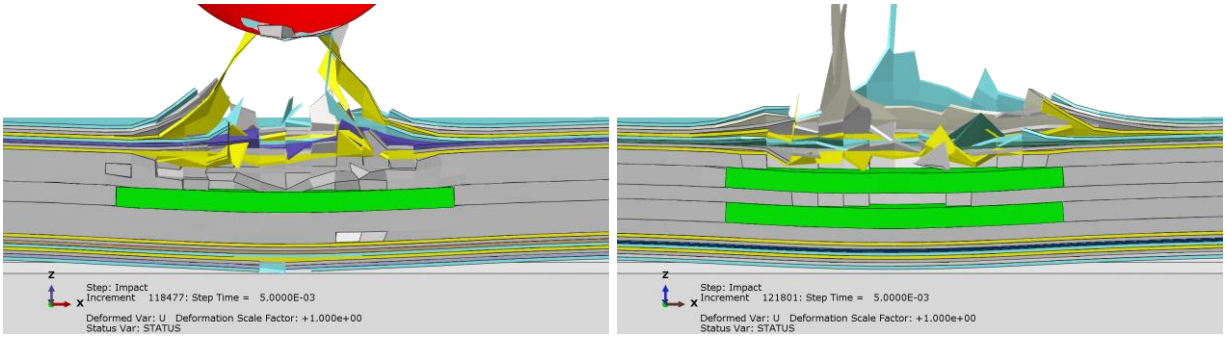

Figure 57: Elliptical shape – deformed shape in central section @ 5.0 ms – left:1 battery; right: 2 batteries

In order to better understand the structural response, the impact force time history is reported in Figure 58 for both models. The model with two batteries is quite stiffer than the one with only one battery as demonstrated also by the previous plots. The upper face of both models undergoes to a severe damage status as well as the core layer between the upper face and the batteries.

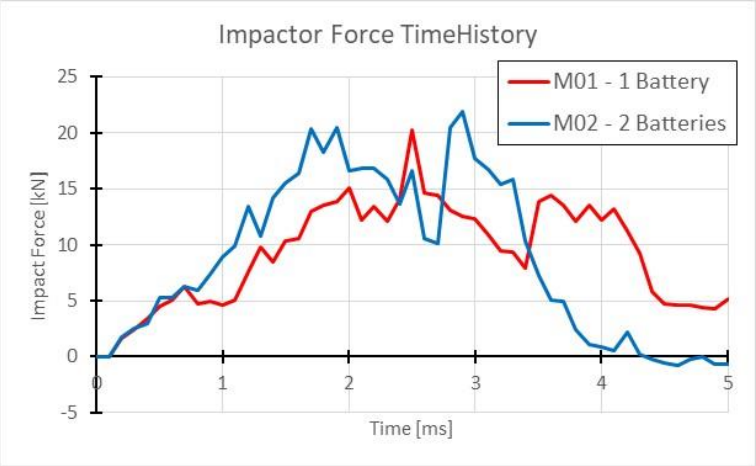

Figure 58: Impact force time history. Comparison between model Configuration A and Configuration B

The bigger damage status of the configuration A can be detected also in the impactor displacement time history (along impact direction), reported in Figure 59.

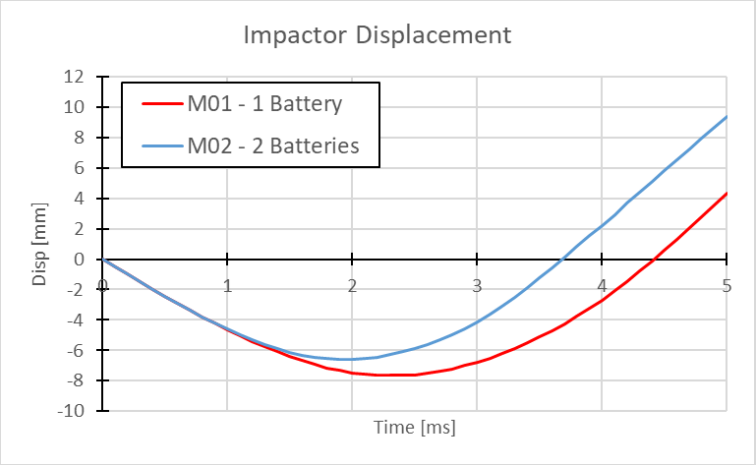

Figure 59: Impactor displacement time-history. Comparison between model Configuration A and Configuration B

From this preliminary study, that should be extended considering also the real cohesive properties, it is possible to observe that increasing the batteries number through the thickness results in a stiffer and a more damage tolerant multifunctional assembly. Indeed, the core, that are much softer than faces, tends to absorb large energy levels in plastic deformation when the component is subjected to forces perpendicular to the plane. This results in a high level of bending in the faces that consequently suffer greater damage.

5. MANUFACTURING OF COUPONS

5.1. COMPOSITE LAMINATES

In the SOLIFLY project, a methodology has been proposed to adapt the curing cycle to the constraints associated to the embedded battery cells. Indeed, the temperature of the curing cycle must be decreased below 160°C to avoid undesirable chemical reactions between the composite part and the electrode of the RMS battery cells. Moreover, due to the presence of liquid electrolyte into the BCE component of the RMS battery cells, the pressure applied during the curing cycle must be decreased. The pressure can be decreased from 7bar to 3.2bar, which is the pressure recommended for sandwich composite materials by the material provider. It is relevant to use that pressure since the battery cells can be considered as core parts into a composite material.

Therefore, a special attention has been paid to the decrease of the maximal temperature in the curing cycle. For that purpose, simulations to estimate the curing rate of the epoxy matrix associated to different curing cycles have been performed in order to determine the optimized curing cycle considering the constraints imposed by the battery cells. Two different models have been considered. The first simple model, proposed by Nelson [10], estimates the evolution of the curing rate of the composite material noted α as a function of time t and temperature T. The second more advanced model has been proposed by Garstka *et al.* [11], that model has been applied successfully to estimate the cure behaviour of the AS4/8552 composite material [11]. Therefore, considering the two models, different curing cycles have been considered with maximal temperature below 160°C and different durations in order to obtain a configuration which presents a curing rate similar to that obtained with the reference cycle at 180°C, as reported in Figure 60a. The curing rates estimated by the Nelson's model and Garstka's model are similar and very close to 1. Finally, the chosen modified configuration consists in maintaining a first plateau at 110°C during 1 hour and then to applied a second plateau at 155°C during 3h, as reported in Figure 60b. The obtained curing rates are respectively equal to α=0.99 for the Nelson's model and α=0.97 for the Garstka's model.

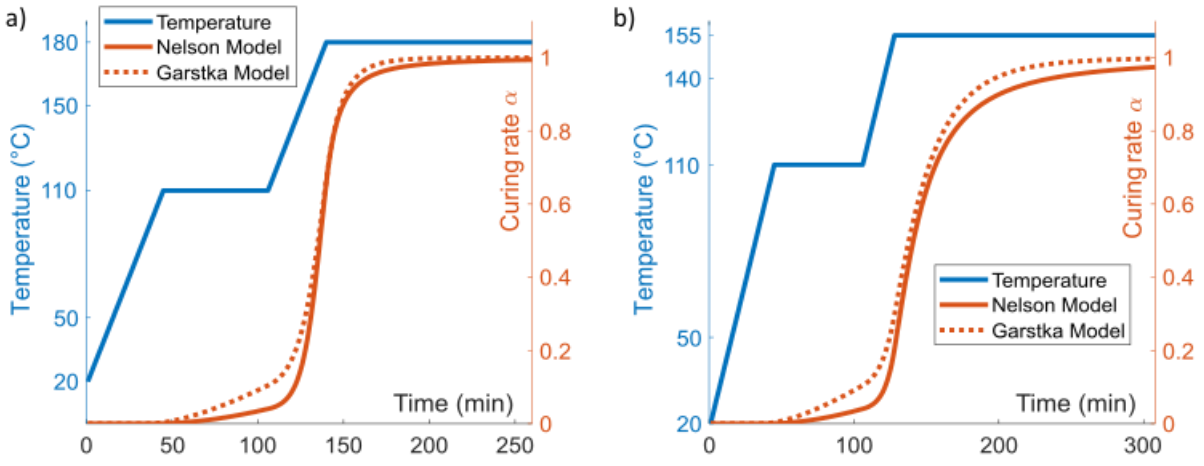

Figure 60: Estimation of the curing rate with the Nelson and Garstka's models for a) the reference and b) the modified curing cycles

Then, it has been decided to manufacture a composite plate with RMS battery cells, as reported in Figure 61, containing 6 battery cells which have been introduced in a quasi-isotropic laminate within the central ±45-plies and 90-plies. The dimensions of the quasi-isotropic laminate are 200 x 30 x 2.92mm. The in-plane size of the battery cells is 100 x 20mm in order to obtain an in-plane section for each battery cells about 2000mm^2. Then, the plate has been again controlled

with X-ray tomography at LMPS Paris-Saclay with two resolutions which are respectively 68μm to observe the whole specimen and 34 μm zooming on the central part around the cells of the specimen. The quality of the composite plate seems to be consistent with our expectancy despite some initial defects mentioned in section 3.2.2. There is no swelling of the central battery cells. We can note that some sliding between the different layers of cells is observed. That point must be improved in the future. Moreover, some short initial delamination cracks seem to be present at the free edges of the battery cells, as reported in Figure 61.

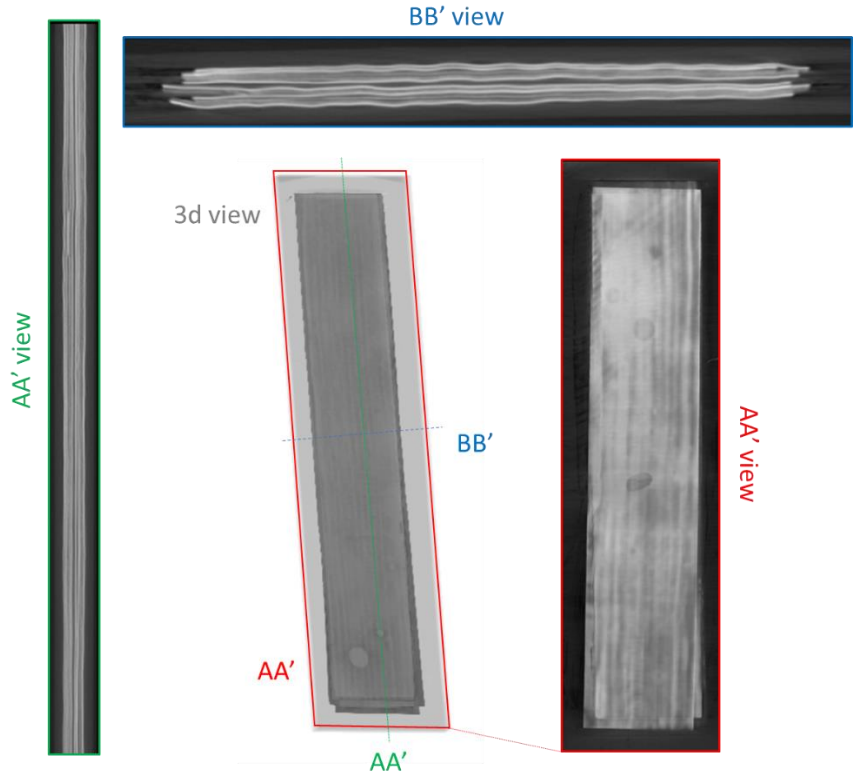

Figure 61: X-Ray tomography of the second manufactured composite plate with 6 embedded battery cells

To conclude, the AS4/8552 composite material is an interesting composite material with high mechanical properties and consistent with the constraints associated to the battery cells after having modified the curing cycle considering moderate temperature and low pressure.

Nevertheless, the manufacturing standard procedures considered in Pipistrel are out-of-autoclave processes without applying any pressure (except that applied by the vacuum bag). Therefore, as suggested by Pipistrel, an AS4/8552 quasi-isotropic composite plate without battery cell has been manufactured without any pressure (except that applied by the vacuum bag) for the MATISSE project. Figure 62 presents a micrograph of a polished free edge where many voids are clearly observed. Considering a binarization method of this micrograph, it is possible to determine the surface void content which is estimated around 22%, what is far higher that the threshold accepted in aeronautics (around 2 or 3%).

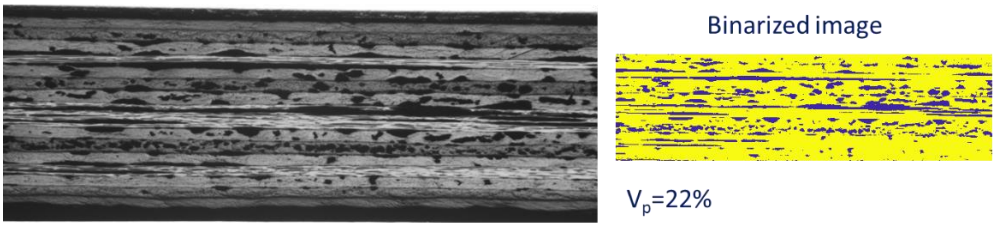

Figure 62: Analysis of one free polished edge of an AS4/8552 composite plate manufactured without any pressure

It means that it is mandatory to consider an autoclave process in the MATISSE project, if the AS4/8552 composite material is chosen. Pipistrel has already found a sub-contractor that can handle that specific point. But the use of an autoclave will limit, in the project, the use of SHM strategies during the curing process. Another strategy could consist in changing the composite material in the MATISSE project. For that purpose, Pipistrel has performed a literature survey of potential other candidates among which the material named IM7/M20 seems to be a good candidate. Indeed, its maximal curing temperature is 130°C, there is not additional pressure to apply during the curing process and the mechanical properties provided by the supplier (Hexcel) seems to be consistent with those of the AS4/8552 material. Onera has contacted Hexcel to obtain more information about the IM7/M20 material which has not yet been widely studied in the literature. This material has been developed mainly for repairing issues and is for now produced only with limited quantities by Hexcel Germany for that topic. Discussions are still performing with Hexcel to determine if the IM7/M20 is a relevant choice for the MATISSE project. It must be noted that if the AS4/8552 material is not chosen, an additional characterization test campaign should be performed in the MATISSE project and therefore, considering a constant funding, the impact test campaign on laminated plates with battery cells should be decreased proportionally.

5.2. SANDWICH LAMINATES

Sandwich laminates are composed of two external face sheets, made of the same material as composite laminates (carbon fiber prepreg), and an internal core, made of foam. For the winglet demonstrator, smart battery cells will be embedded into the core.

In case of structural battery cells integrated into the face sheets, the process is as explained previously in Section 5.1.

The preliminary manufacturing process of sandwich laminates integrated with structural battery cells into the core is as follows:

1. Perform the conditioning of the mould.
2. Place the required number of carbon fiber prepreg plies with the required orientation.
3. Make a cut-out on the foam with the size of battery cells and remove from the foam the same thickness as the battery cells that will be embedded into it. Cut in plane as many times as battery stacks.
4. Place the foam. Initially it is assumed that is not necessary to glue it to the face sheet, since the epoxy resin in the prepreg is enough for adhesion.
5. With the cut-out pieces, firstly place foam and then battery cells and foam in the required sequence, finishing with a layer of foam. Apply an epoxy adhesive between layers and on the borders of foam. Place the cables from battery cells between the face sheet and core.
6. Place the required number of carbon fiber prepreg plies with the required orientation.
7. Install the vacuum bag and follow the specified curing requirements and demoulding process.

Figure 63 illustrates the process of a conventional sandwich composite:

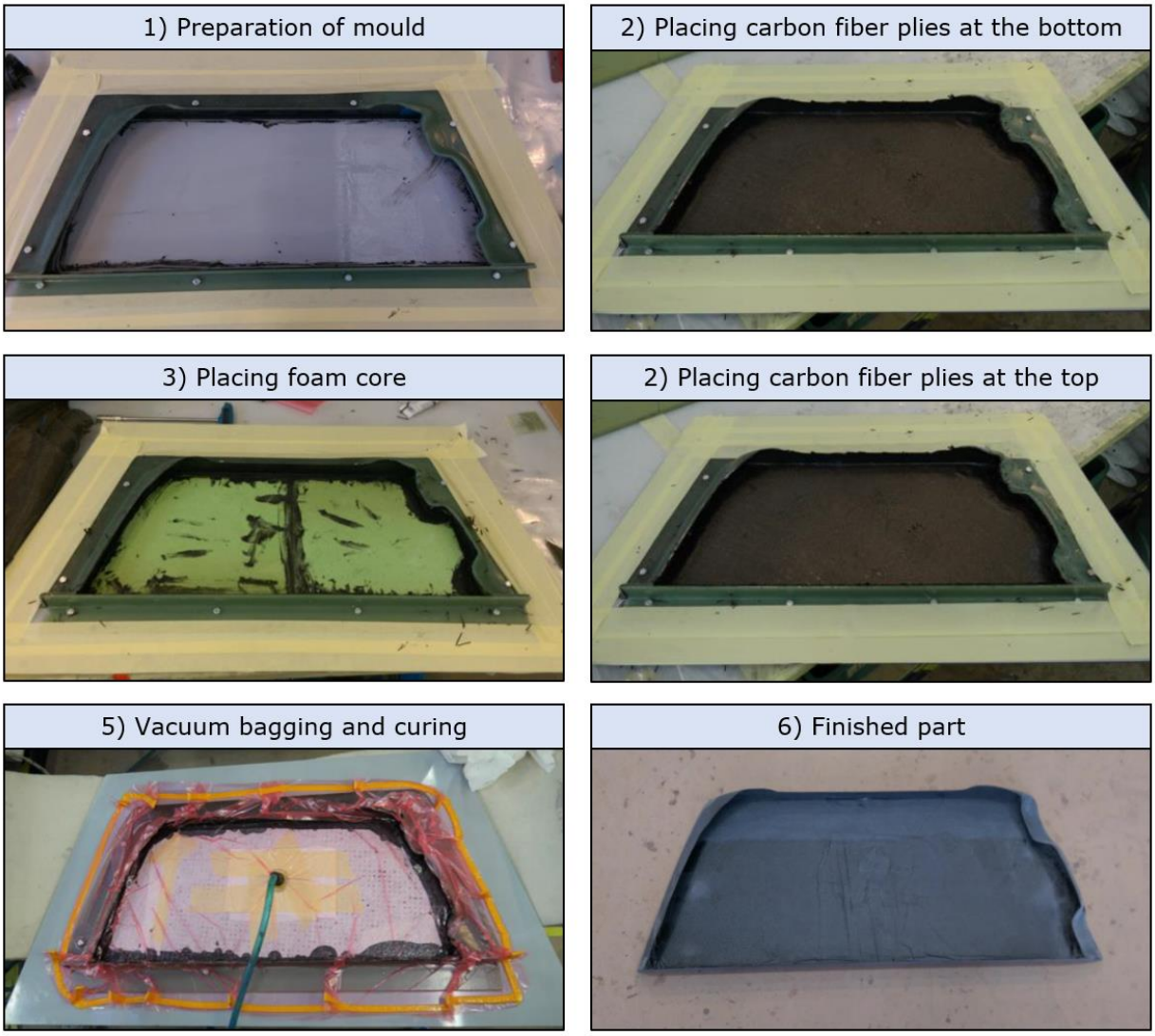

Figure 63: Manufacturing process of a conventional sandwich composite part

6. MATERIAL FOR WINGLET DEMONSTRATOR DEVELOPMENT

Determination of requirements for the material of winglet demonstrator has been based on the experience obtained in SOLIFLY. The curing temperature must be below 160°C, at which battery cells begin to be degraded. It is preferable the use of unidirectional fibers, since they provide a better interface with structural batteries. On the other hand, the use of woven fabric would require more development effort. Regarding the technology of the material, between the options of wet lamination and prepreg, it is preferable the second one in order to reduce the complexity of manufacturing. In addition, public mechanical properties are more frequently available for prepreg materials than for wet laminated composites.

During the curing cycle, temperature sensors are needed for health monitoring of battery cells. It was identified that autoclave curing might be problematic for this purpose since it is required that sensors are connected to instrumentation outside the oven, which must be totally sealed from the exterior to allow pressurisation. It is feasible to find available autoclave ovens which allow to connect instrumentation, but they are meant for small parts as plates for testing, and not large enough for the winglet demonstrator, so this would impede the use of sensors for monitoring.

The following table show the main characteristics of the carbon fiber material candidates for the winglet demonstrator:

Table 5 – Carbon fiber material candidates

Material	Type	Technology	Properties available	Autoclave	Curing temperature
Hexcel AS4/8552	Unidirectional	Prepreg	Yes	Yes	180°C (reduced to 155°C)
Hexcel IM7/M20	Unidirectional	Prepreg	Partial	No	130°C
Pipistrel material	Woven 0/90°	Wet lamination	Partial	No	80°C

The winglet on which MATISSE demonstrator is based, is made of wet laminated woven fiber and epoxy composite. This material is not ideal for the project but it will remain as a backup option to remove the risk of not finding a suitable material.

As explained in Section 5.1, AS4/8552 is the material used in SOLIFLY, which has excellent mechanical properties, and its curing temperature was successfully reduced to allow the use of structural batteries. However, this curing temperature is close to the lower bound (150°C) at which the prepreg is not fully cured. The small range of valid temperatures it was considered as a risk for suitability of the material for manufacturing, since the wingtip curing requires a gradient of temperatures from exterior to interior of the component, and that gradient in actual production is usually higher than the experimented 10°C between minimum curing and battery cells degradation temperatures.

Pipistrel has performed a literature survey of potential other candidates among which the material named IM7/M20 seems to be a good candidate. Indeed, its maximal curing temperature is 130°C, there is not additional pressure to apply during the curing process and the mechanical

properties provided by the supplier (Hexcel) seems to be consistent with those of the AS4/8552 material. Hexcel has been contacted to obtain more information considering the cost and the delay associated to the IM7/M20 material which has not yet been widely studied in the literature. This material is for now mainly developed in Germany for repairing issues.

For sandwich core, the foam must resist the curing temperature of the solid laminate. After final selection of the carbon fiber composite, an appropriate core will be chosen from the following table:

Table 6 – Sandwich core material candidates

Material	Density [kg/m^3]	Max. curing temperature [°C]
Airex C71.75	80	140
Divinycell HT81	80	145
Rohacell IG-F series	32 - 110	130
Rohacell SL series	75 - 205	170 - 180
Rohacell WF series	52 - 300	180

7. CONCLUSIONS

The present deliverable reports the results achieved so far in the framework of WP3 aiming at developing a design methodology to integrate SB cells into both monolithic and sandwich laminates by optimizing mechanical performance and electrochemical storage capacity.

Advanced integrated models and simulations have been performed at coupon level (with and without battery cells) subjected to both quasi-static and low velocity/low energy impact loads. A dedicated numerical procedure has been created to predict and simulate the damage onset and propagation in laminates with embedded battery cells. Smart SB battery cells have been modelled also into the foam core of sandwich laminates between the two laminate face sheets to properly manage impact and bending loadings.

The preliminary results of the project focused on modelling battery cells embedded in composite laminated plates and evaluating the resulting mechanical performance. The proposed modelling has been applied to a structural battery specimen integrating two multi-electrode-layer battery cells in the central 90 plies and ±45 plies. The influence of the nonlinear behaviour of the battery cells has shown to be non-negligible. Considering the battery cells included in the composite laminated plate, the predicted macroscopic modulus has been decreased about 3% considering an elastic behaviour for the battery cells and 4% considering the plastic behaviour. Also, although the evolution of the onset of transverse cracks is not modified, the battery cells should fail for an applied macroscopic strain equal to 0.6% (leading to a decrease of the first damage event recorded during the test). Finally, the macroscopic stress at failure is decreased by 4% considering the elastic behaviour for the battery cells and 8% considering plasticity. Such conclusions shall be considered applicable for tension loadings.

The evaluation of the mechanical response under dynamic loads has been carried out in accordance with the standard ASTM 7136 for both solid and sandwich laminates by using an explicit solver with reasonable computational cost and good accuracy level. For the sandwich specimen, the core was simulated as a Rohacell 300WF foam with total thickness of 5mm. Results have confirmed that the global stiffness of the multifunctional sandwich assembly increases with the number of battery cells through the thickness, thus resulting in a more damage tolerant structural battery.

Regarding the manufacturing technology, the AS4/8552 composite material has shown to be a viable composite material with adequate mechanical properties, even when the curing cycle has been modified by considering moderate temperature (below 160°C to avoid undesirable chemical reactions between the composite part and the electrode of the RMS battery cells) and low pressure. The overall decrease in the mechanical properties of the manufactured samples can be limited by improving the manufacturing process and thus the quality of the composite part around the battery cells. However, additional work needs to be carried out for bending loads which will be the loading applied to final demonstrator of the MATISSE project.

In view of the wingtip demonstrator manufacturing, a literature survey has been performed to assess also other potential material candidates having mechanical properties consistent with those of the AS4/8552 material. The IM7/M20 material appears a good option since it requires maximal curing temperature equal to 130°C and there is not additional pressure to apply during the curing process.

8. REFERENCES

[1] SOLIFLY - Semi-SOlid-state LI-ion batteries FunctionalLY integrated in composite structures for next generation hybrid electric airliner (CleanSky2 , GA 101007577, 2021-2023), (n.d.). https://cordis.europa.eu/project/id/101007577.

[2] F. Laurin, A. Beutl, Q. Jiang, H. Kühnelt, Concepts for integrating electrical energy storage into CFRP laminate structures for aeronautic applications, J. Phys. Conf. Ser. 2526 (2023) 012062. https://doi.org/10.1088/1742-6596/2526/1/012062.

[3] M. Wan, D. Bresser, A. Beutl, R. Simmarano, MATISSE: Deliverable D2.1 - Interim report on electrochemical material selection, initial cell design, on-cell sensor development, 2023.

[4] F. Laurin, N. Carrere, J.F. Maire, A multiscale progressive failure approach for composite laminates based on thermodynamical viscoelastic and damage models, Compos. Part Appl. Sci. Manuf. 38 (2007) 198–209.

[5] Z. Hashin, Failure criteria for unidirectional fiber composites, J. Appl. Mech. 47 (1980) 329–334.

[6] C. Fougerouse, Understanding and modelling of the effects of out-of-plane waviness defects on the mechanical performance of a thermoplastic matrix laminate, université paris-Saclay, 2022.

[7] A.H. Baluch, O. Falco, J.L. Jimenez, B.H. Tijs, C.S. Lopes, An efficient numerical approach to the prediction of laminate tolerance to Barely Visible Impact Damage, Compos. Struct. 225 (2019) 111017.

[8] M. Nicol, Compréhension et modélisation de l'influence de l'ordre d'empilement sur les scénarios d'endommagement dans des composites stratifiés de plis unidirectionnels, Université de Paris Saclay, 2023.

[9] J. Besson, G. Cailletaud, J.L. Chaboche, S. Forest, Mécanique non linéaire des matériaux, 2001.

[10] P.H. Nelson, Permeability-Porosity Relationships in Sedimentary Rock, Log Anal. (1994).

[11] T. Garstka, N. Ersoy, K.D. Potter, M.R. Wisnom, In situ measurements of through-the-thickness strains during processing of AS4/8552 composite, Compos. Part A. 38 (2007) 2526.